CrystEngComm

Accepted Manuscript

CrystEngComm RSCPublishing

HIGHLIGHT

Cite this: DOI: 10.1039/x0xx00000x

Received 00th XXX 2015,
Accepted 00th XXX 2015

DOI: 10.1039/x0xx00000x

www.rsc.org/

Significant developments on rare-earth-containing polyoxometalate chemistry: synthetic strategies, structural diversities and correlative properties

Xing Ma, Wen Yang, Lijuan Chen* and Junwei Zhao*

Owing to their unique and abundant structures and potential multi-fold applications in various fields such as luminescence, magnetism, catalysis etc, rare-earth-containing polyoxometalates (RECPs) play an important role in the development of polyoxometalate chemistry. In this article, the major progresses in RECPs made in the past decade involving synthetic strategies, structural characteristics and some significant properties related to optics, catalysis and magnetism are highlighted and discussed. The final section is committed to looking forward to some future perspectives in this field and providing some personal insights or viewpoints for the ongoing trends in the future.

1. Introduction

Polyoxometalates (POMs) are the discrete anionic clusters that can be condensed by oxo-bridged early transition metal atoms in their high oxidation states (usually Mo^{VI}, W^{VI}, V^{V}, Nb^{V} or Ta^{V}).[1] These metal atoms are coordinated by six oxygen ligands giving rise to $\{MO_6\}$ octahedral geometries and then the resulting $\{MO_6\}$ units are further joined together by corner-, edge- (rarely face-) sharing oxygen atoms (formally O^{2-} or occasionally HO^{-} ions).[2] With regard to polyoxoanions (POAs), several classical types have been reported: Keggin, Well-Dawson, Lindqvist, Anderson-Evans, Weakley, Silverton, Stranberg, etc.[3] After Pope and Müller published a review article that comprehensively elucidated the fascinating structural characteristics and important potentials in several disciplines of POMs in 1991,[4] a myriad of unexpected POM structures came to constantly emerging. Then a special thematic issue on POMs organized by Hill in 1998 not only rapidly accelerated the discovery of peculiar POM species, but also provoked the emerge of some new research areas in POM chemistry.[5] The flexible and diversiform structures endow POM-based materials many versatile performances in various areas such as catalysis, medicine, materials science, nanotechnology, molecular magnetism and photochemistry.[6] Hitherto, synthesis and preparative chemistry on POMs still remain a great driving force in exploring and discovering novel POM-based materials despite the first POM $(NH_4)_3PMo_{12}O_{40}$ was discovered by Berzelius as early as 189 years ago and even the first structural determination of the phosphotungstic acid $H_3[PW_{12}O_{40}]\cdot 29H_2O$ was accomplished until 1936 by Keggin by virtue of the powder X-ray diffraction study.[7]

Based on their nucleophilic oxygen-enriched surfaces, POM units can act as excellent inorganic multidentate candidates to integrate transition-metal (TM), rare-earth (RE) or both into their structures.[8] Thereby, a vast array of novel TM, RE or TM–RE-containing POMs have being dug out gradually. For example, the first RE-containing POM (RECP) $(NH_4)_2[H_6CeMo_{12}O_{42}]\cdot nH_2O$ was discovered by Barbieri in 1914.[9] Then in 1971, Peacock and Weakley successfully separated a family of 1:2 series RECPs $[RE(W_5O_{18})_2]^{9-}$, $[RE(SiW_{11}O_{39})_2]^{13-}$ and $[\alpha_2\text{-}RE(P_2W_{17}O_{61})_2]^{17-}$, which are a milestone in the history of RECPchemistry.[10] Historically, the first TM substituted POM (TMSP) was communicated by Simmons

Xing Ma was born in Anhui, China in 1995 and now she is pursuing her BS degree in chemistry at Henan University. In 2013, she as a student began to conduct scientific research in the group of Prof. Junwei Zhao in Henan Key Laboratory of Polyoxometalate Chemistry. Her current research interest is focused on the designed synthesis and luminescent properties of organic-inorganic hybrid rare-earth-containing polyoxometalate materials.

Wen Yang was born in Henan Province, China. Currently, she is majoring in materials chemistry to receive the BS degree at Henan University and works as a student in Henan Key Laboratory of Polyoxometalate Chemistry under the supervision of Prof. Junwei Zhao. Her current research is concentrated on the preparation and electrochemical properties of novel rare-earth substituted

polyoxometalate aggregates.

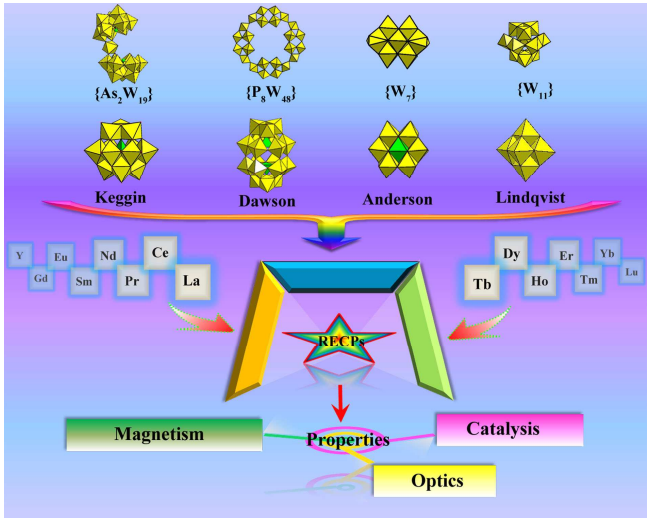

Scheme 1 Schematic representation of the assembly processes of RECPs. Several typical POAs and three significant properties are highlighted.

at the 1962 (Stockholm) International Conference on Coordination Chemistry (ICCC) and its structure (it is an 11-tungstosilicate wherein one W atom of the Keggin structure was replaced by a Co^{2+} ion) was confirmed by St. Moritz at the 1966 ICCC.[11] Moreover, the composition, size, shape, solubility, redox potential, magnetic and catalytic properties of TMSPs are relatively easy to be fine-tuned by elaborate selection of types and oxidation states of TM ions.[12] Therefore, the development of TMSPs is much faster than that of RECPs. However, RECPs can exhibit special luminescent, Lewis acid catalytic or magnetic functionalities by taking advantage of the electronic and structural features of RE ions (Scheme 1):[13] (i) Depending on the special electronic properties of lanthanide (Ln) cations (the shielding of the 4f orbitals by the filled $5s^25p^6$ subshells), Ln-containing compounds often have good fluorescence activity and long lifetime, which makes them be used in optical fields such as light-emitting diodes, plasma displays, sensory probes, medicinal

Lijuan Chen was born in Henan, China. She gained her BS and MS degrees in chemistry from Henan University (2005) and obtained her PhD under the supervision of Prof. Jianmin Chen at Lanzhou Institute of Chemical Physics, Chinese Academy of Sciences (2009). In 2009, she joined Henan University and was appointed as a Lecture. In 2013, she was promoted to an Associate Professor. Since April 2014, she has been working with Prof. Jingyang Niu as a postdoctoral fellow in Henan University. Her research interest is focused on coordination chemistry of polyoxometalate chemistry and photophysical properties of polyoxometalate-based materials.

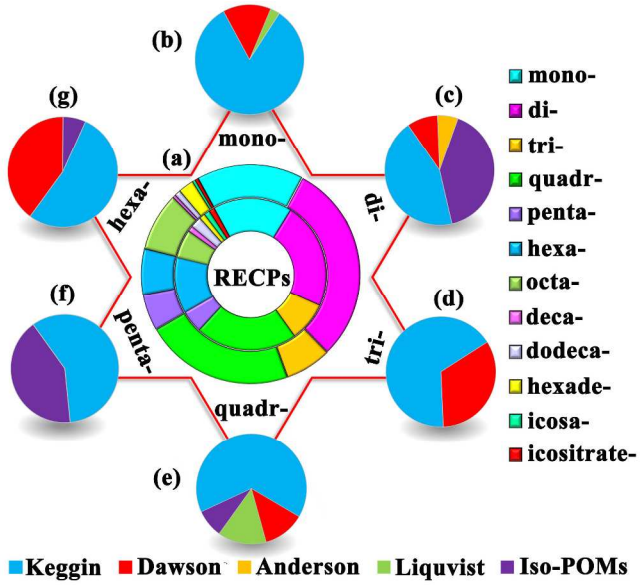

Fig. 1 (a) The inner ring represents the number of reported papers (sum: 83) while the outer ring represents the number of as-synthesized RECPs (sum: 221) between 2005 and 2015. (b) The percentages of different structural types in mononuclear RECPs: MKRECPs: 82.8%, MDRECPs: 14.3%, MLRECPs: 2.9%. (c) The percentages of different structural types in dinuclear RECPs: DKRECPs: 43.9%, DDRECPs: 9.1%, DARECPs: 6.1%. (d) The percentages of different structural types in trinuclear RECPs: TKRECPs: 66.7%, TDRECPs: 33.3%. (e) The percentages of different structural types in quadrnuclear RECPs: QKRECPs: 65.3%, QDRECPs: 12.2%, QLRECPs: 12.2%. (f) The percentages of different structural types in pentanuclear RECPs: PKRECPs: 58.3%. (g) The percentages of different structural types in hexanuclear RECPs: HKRECPs: 53.3%, HDRECPs: 40%.

analyses, monitoring drug delivery as well as cell imaging;[14] (ii) high coordination numbers and flexible coordination geometries of RE ions

Junwei Zhao obtained the BS degree in chemistry in 2002 and gained his MS degree under the supervision of Prof. Jingyang Niu in 2005 from Henan University. In 2008, he received his PhD under the supervision of Prof. Guo-Yu Yang at Fujian Institute of Research on the Structure of Matter, Chinese Academy of Sciences. After then, he joined Henan University, was promoted to a full Professor in chemistry in 2014 and was ranked as an academic leader of Department of Education of Henan Province in 2015. He is mainly engaged in the synthesis and preparative chemistry of polyoxometalate-based functional materials and the relevant optical, electrical, magnetic and medical properties.

endow them with the ability of leaving some residual coordination sites that can act as the effective Lewis acids for the activation of substrates.[13e] It has proved that the introduction of some RE ions (Lewis acidic cations) into POM skeletons can form recoverable catalysts with high chemoselectivities.[13c] On the other hand, oxyphilic RE ions can easily combine with oxygenic ligands (such as POM fragments herein) that are guided by the Hard and Soft Acids and Bases (HSAB) theory;[15] (iii) On account of the presence of the large number of unpaired 4f electrons, RE ions are widely utilized to manufacture molecule-based magnetic materials.[16] Hence, RECPs have always been a sparkling and important subclass in the large family of POMs. Moreover, the emergence of some novel high-nuclear RECPs in the past decade has also aroused the worldwide increasing attention on high-nuclear RECP chemistry.[17]

In this highlight article, we will begin to give the intensive accounts on some typical RECPs obtained in the past decade according to the number of RE cations and the structure types of POAs per molecular unit (Fig. 1). The synthetic strategies, structural characteristics and some important properties will be simultaneously involved in this highlight article. We hope this highlight article to be able to provide some useful highlights for designing and synthesizing novel RECPs with neoteric structures and wonderful properties in the following time.

2. Results and discussion

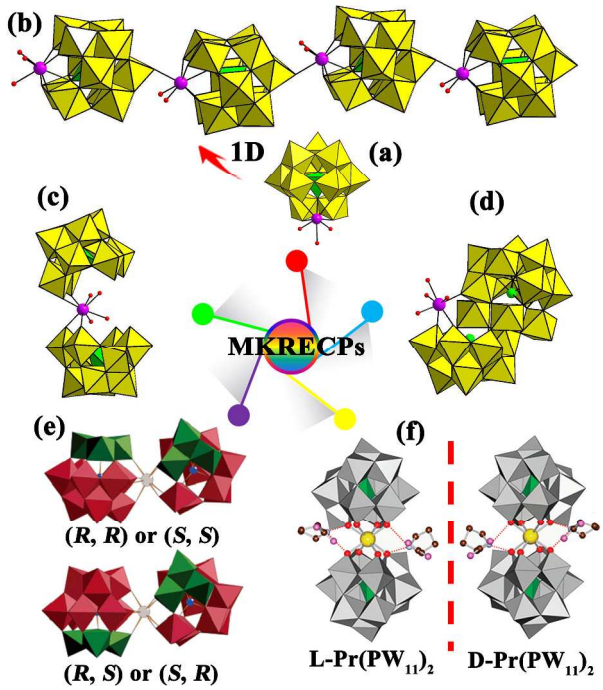

Fig. 2 (a) The $[\alpha\text{-GeW}_{11}O_{39}Y(H_2O)_2]^{5-}$ building block. (b) The 1-D chain formed by $[\alpha\text{-GeW}_{11}O_{39}Y(H_2O)_2]^{5-}$ units. (c) View of $[\{RE(H_2O)_4\}(\gamma\text{-SiW}_{10}O_{36})_2]^{13-}$. (d) View of $[RE(H_2O)_4Sb_2W_{21}O_{72}(OH)]^{10-}$. (e) Two possible isomers of the structural unit of $[Ln(\beta_2\text{-SiW}_{11}O_{39})]_2]^{13-}$ (Copied from ref. 25). (f) View of enantiopure $K_{1.3}Na_{3.2}H_{6.5}[L\text{-Pr}(PW_{11}O_{39})_2]\cdot 8.3L\text{-proline}\cdot 21.5H_2O$ and $K_{1.3}Na_{3.2}H_{6.5}[D\text{-Pr}(PW_{11}O_{39})_2]\cdot 8.3D\text{-proline}\cdot 17H_2O$ (Copied from ref. 26). (WO_6: yellow, XO_4: bright green, RE: light purple, O: red)

2.1 Mononuclear RECPs

2.1.1 Mononuclear Keggin-type RECPs (MKRECPs)

It is generally known that the removal of a {M=O} group can make the Keggin-type $[XM_{12}O_{40}]^{n-}$ skeleton transform to a $[XM_{11}O_{39}]^{m-}$ fragment with a larger "bite angle" defect site, which can clench a metal ion into the defect site. Meanwhile, the high coordination RE ion inserted into the vacant site of the monovacant $[XM_{11}O_{39}]^{m-}$ moiety can provide several (usually 2–4) additional available coordination sites and further are used as linkers to combine one or more other lacunary POM units together. Since Peacock and Weakley first isolated the sandwich-type $[RE(SiW_{11}O_{39})_2]^{13-}$ POAs, a large number of mononuclear RECPs have been unremittingly reported. For the long period, Peacock–Weakley type MKRECPs (1:2-type) with discrete structures have dominated the mainstream status in the realm of MKRECPs.[18,12] Until 2001, Pope et al. for the first time communicated two 1-D zigzag chains based on 1:1-type $[RE(\alpha\text{-SiW}_{11}O_{39})(H_2O)_3]^{5-}$ (RE = Ce^{III}, La^{III}) MKRECP units.[19] After that, several kinds of special MKRECPs with extended structures have been obtained.[20] By virtue of the nature of different RE cations, Mialane and coworkers not only synthesized a 1-D zigzag chainlike MKRECP $[Eu(\alpha\text{-SiW}_{11}O_{39})(H_2O)_2]^{5-}$ but also isolated a 1-D linear MKRECP $[Yb(\alpha\text{-SiW}_{11}O_{39})(H_2O)_2]^{5-}$.[20a] Inspired by the previous innovative work, Niu's group addressed a novel 1-D chain MKRECP built by $[\alpha\text{-SiW}_{11}O_{39}Pr(H_2O)_4]^{5-}$ units via $[NaPr_2(H_2O)_{12}]^{7+}$ bridges.[20b] With the further exploration, they reported a novel 1-D zigzag chain architecture based on $[\alpha\text{-GeW}_{11}O_{39}Y(H_2O)_2]^{5-}$ in 2006 (Fig. 2a, 2b),[20d] which is different from Pope's work. Besides, in the past decade, some other discrete MKRECPs have also been synthesized.[21] As more {M=O} groups can lose from the Keggin POA, the negative charge of the resulting vacant POA can increase, which renders the vacant POA to become more nucleophilic and endows them higher reactivity to bind with RE ions.[2] In 2013, by reaction of divacant precursor $TBA_4H_4[\gamma\text{-SiW}_{10}O_{36}]$ with $[RE(acac)_3]$ (RE = Dy^{III}, Gd^{III}, La^{III}; acac = acetylacetonate) in a mixed acetone–water solvent system, Mizuno et al synthesized a new type of sandwich-type MKRECP with vacant sites $[\{RE(H_2O)_4\}(\gamma\text{-SiW}_{10}O_{36})_2]^{13-}$ (Fig. 2c), in which the vacant sites are surrounded by coordinating W–O and Ln–O oxygen atoms.[22] In the same year, Kortz's group prepared the mono-RE derivatives of the Krebs-type 22-tungsto-2-antimonate $[RE(H_2O)_4Sb_2W_{21}O_{72}(OH)]^{10-}$ (RE = Yb^{III}, Lu^{III}) (Fig. 2d) by reaction of RE ions with $[Sb_2W_{22}O_{74}(OH)_2]^{12-}$ in aqueous acidic (pH 5) medium.[23] It is rather intriguing that $[RE(H_2O)_4Sb_2W_{21}O_{72}(OH)]^{10-}$ contains two $[B\text{-}\alpha\text{-SbW}_9O_{33}]^{9-}$ fragments joined by two tungsten ions, leading in the lacunary $[Sb_2W_{20}O_{70}]^{14-}$ unit, which is then coordinated to a RE ion and a tungsten atom, giving rise to an architecture with idealized C_s symmetry (Fig. 2d). On the other hand, recently, the exploration and preparation of chiral MKRECPs has become an emerging field in POM chemistry because of the flexible rotation of the $[XM_{11}O_{39}]^{m-}$ moiety and intriguing 4f–4f transitions of RE ions, thus, chiral $[RE(XW_{11}O_{39})_2]^{n-}$ POAs have attracted increasing interest due to potential applications in asymmetric catalysts, chiral recognition and biological fields.[24,13e] Kortz et al. used the reaction of RE ions with the chiral monovacant Keggin-type $[\beta_2\text{-SiW}_{11}O_{39}]^{8-}$ precursor in a 1:2 molar ratio in KCl medium at pH 5 and separated a series of chiral MKRECPs $[RE(\beta_2\text{-SiW}_{11}O_{39})_2]^{13-}$ (RE = La^{III}, Ce^{III}, Sm^{III}, Eu^{III}, Gd^{III}, Tb^{III}, Yb^{III}, Lu^{III}) (Fig. 2e), which represent the first RECPs based on chiral $[\beta_2\text{-SiW}_{11}O_{39}]^{8-}$ fragments.[12] Results indicate that large RE ions

seem to be favorable to an (R,R) or (S,S) configuration of the Keggin units with an increasing amount of (R,S) or (S,R) configuration found in the solid state as the RE ion decreases in size.[25] Different from Kortz's method, Naruke and collaborators utilized chiral amino acids (L- and D-proline) as the chirality transfer agents to made the chiral phosphotungstate-based MKRECPs $K_{1.3}Na_{3.2}H_{6.5}[L\text{-}Pr(PW_{11}O_{39})_2]\cdot 8.3L\text{-proline}\cdot 21.5H_2O$ and $K_{1.3}Na_{3.2}H_{6.5}[D\text{-}Pr(PW_{11}O_{39})_2]\cdot 8.3D\text{-proline}\cdot 17H_2O$ (Fig. 2f) and also investigated their optical activities by the circular dichroism (CD) spectra.[26] Similarly, we also obtained an acentric phosphotungstate $KNa_3[HPro]_7[Sm(\alpha\text{-}PW_{11}O_{39})_2]\cdot Pro\cdot 18H_2O$ (Pro = D-proline) by means of the chirality transfer strategy and preliminarily studied its ferroelectric properties.[21c]

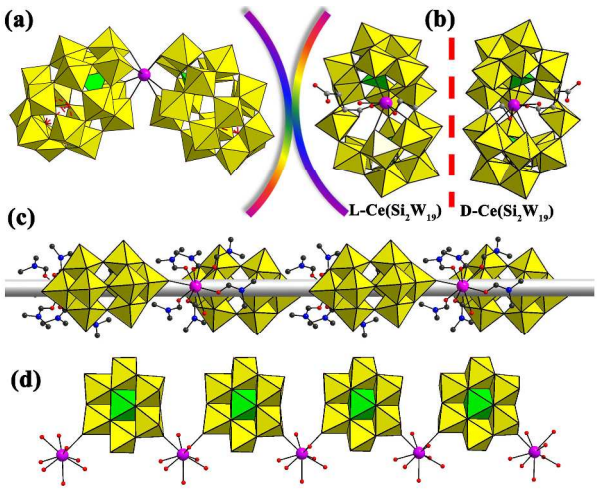

Fig. 3 (a) The structure of $[Ce\{X(H_4)W_{17}O_{61}\}_2]^{19-}$. (b) Views of two enantiomerically pure polytungstates $Na_2[(CH_3)_2NH_2]_3\{Na\subset[Ce^{III}(H_2O)(CH_3CH_2OH)(L\text{-}tartH_3)(H_2Si_2W_{19}O_{66})]\}\cdot 3.5H_2O$ [L-Ce(Si_2W_{19})] and $[(CH_3)_2NH_2]_7\{Na\subset[Ce^{III}(H_2O)(CH_3CH_2OH)(D\text{-}tartH_3)(Si_2W_{19}O_{66})]\}\cdot 2.5H_2O$ [D-Ce(Si_2W_{19})]. (c) The 1-D helical chain of $[Ce(H_2O)(DMF)_6(W_{10}O_{32})]\cdot DMF\cdot CH_3CH_2OH$. (d) View of the 1-D zigzag chain of $[La(H_2O)_7Al(OH)_6Mo_6O_{18}]_n\cdot 4nH_2O$. ($WO_6$ and MoO_6: yellow, XO_4: bright green, RE: light purple, O: red, C: cray, N: blue)

2.1.2 Mononuclear Dawson-type RECPs (MDRECPs)

In comparison with those abundant MKRECPs, sporadic MDRECPs were also made. In 2005, Pope et al. isolated two λ-shaped MDRECPs with a syn C_2 conformation $[Ce(XH_4W_{17}O_{61})_2]^{19-}$ (X = P^V, As^V) by reaction of the $[H_4XW_{18}O_{62}]^{7-}$ POA and the Ce^{3+} cation.[27] This λ-shaped MDRECP anion is constructed from two monovacant Dawson-like polyoxotungstate fragments $[XH_4W_{17}O_{61}]^{11-}$ anchoring a Ce^{3+} cation (Fig. 3a), in which the "empty" $\{O_4\}$ tetrahedra are in the remote positions of the Ce^{3+} cation.[27] In 2014, our group also reported a λ-shaped Dawson-like Ce^{IV}-hybridizing selenotungstate with a syn C_2 conformation $[Ce(SeW_{17}O_{59})_2]^{20-}$.[28] Notably, the main difference between $[Ce(XH_4W_{17}O_{61})_2]^{19-}$ and $[Ce(SeW_{17}O_{59})_2]^{20-}$ lies in the fact that the tetrahedral geometry of the As^V (P^V) atoms in the former and the trigonal pyramid geometry of the Se^{IV} atom in the latter lead to the distinction of the number of oxygen atoms in Dawson-like $[XH_4W_{17}O_{61}]^{11-}$ and $[SeW_{17}O_{59}]^{12-}$ fragments. In 2014, Xu et al obtained two enantiomerically pure polyoxotungstates $Na_2[(CH_3)_2NH_2]_3\{Na\subset[Ce^{III}(H_2O)(CH_3CH_2OH)(L\text{-}tartH_3)(H_2Si_2W_{19}O_{66})]\}\cdot 3.5H_2O$ and $[(CH_3)_2NH_2]_7\{Na\subset[Ce^{III}(H_2O)(CH_3CH_2OH)(D\text{-}tartH_3)(Si_2W_{19}O_{66})]\}\cdot 2.5H_2O$ ($tartH_4$ = tartaric acid) by reaction of the trivacant Keggin $[\alpha\text{-}SiW_9O_{34}]^{10-}$ and L-(+)-cerium tartrate or D-(–)-cerium tartrate (Fig. 3b).[29] More interestingly, chiral tartrate ligands directly are combined with the unprecedented vacant $[Si_2W_{19}O_{66}]^{10-}$ segments. Moreover, Z-scan result illustrates that two enantiomerically pure polyoxotungstates are the first chiral POMs that show two-photon absorption properties typical of the third-order nonlinear optical response.

2.1.3 Mononuclear Anderson-type RECPs (MARECPs)

Due to the low surface charges of Anderson POAs, reports on MARECPs in the past decade are very rare. However, in 2002, Das and co-workers reported a 1-D zigzag chain-like MARECP $[La(H_2O)_7Al(OH)_6Mo_6O_{18}]_n\cdot 4nH_2O$ based on Anderson-type $[Al(OH)_6Mo_6O_{18}]^{3-}$ units and RE connectors (Fig. 3d).[30] Another series of 1-D chain-like MARECPs $[RE(H_2O)_7Cr(OH)_6Mo_6O_{18}]_n\cdot 4nH_2O$ (RE = La^{III}, Gd^{III}) and $[RE(H_2O)_7Al(OH)_6Mo_6O_{18}]_n\cdot 4nH_2O$ (RE = Gd^{III}, Eu^{III}) were obtained by their group in 2014.[31] This work fills a vacancy of the Anderson-type species in the field of mononuclear RECPs.

2.1.4 Mononuclear Lindqvist-type RECPs (MLRECPs)

In the classical Lindqvist POM family, the typical decatungstate $[W_{10}O_{32}]^{4-}$ isopolyanion can be considered as two monovacant Lindqvist $[W_5O_{14}]^{2-}$ units linked by four corner-sharing oxygen atoms. To date, relevant reports on MLRECPs are very rare. Luo et al utilized the assembly of decatungstate $[W_{10}O_{32}]^{4-}$ units and $[Ce(H_2O)(DMF)_6]^{4+}$ cations and successfully separated a novel 1-D MLRECP $[Ce(H_2O)(DMF)_6(W_{10}O_{32})]\cdot DMF\cdot CH_3CH_2OH$ (DMF = dimethyl formamide),[32] in which each $[Ce(H_2O)(DMF)_6]^{4+}$ is covalently bonded to two $[W_{10}O_{32}]^{4-}$ units via corner-sharing oxygen atoms generating an infinite 1-D helical chain (Fig. 3c).

2.2 Dinuclear RECPs

2.2.1 Dinuclear Keggin-type RECPs (DKRECPs)

Exactly as MKRECPs in the family of mononuclear RECPs, DKRECPs also hold the dominant position in the realm of dinuclear RECPs. In terms of purely inorganic DKRECPs, the reported structures are kaleidoscopic. For instance, in 2009, Niu's group separated the novel phosphotungstate-based DKRECPs $[\{(\alpha\text{-}PW_{11}O_{39}H)RE(H_2O)_3\}_2]^{6-}$ (RE = Nd^{III}, Gd^{III}) (Fig. 4a), where two mono-RE substituted Keggin $[\alpha\text{-}PW_{11}O_{39}RE(H_2O)_3]^{4-}$ subunits are bridged by two RE–O–W linkers to form the first 2:2-type monovacant Keggin phosphotungstate dimers.[33] Through the stepwise incorporation strategy of two different RE cations into the vacant sites of POMs, Mizuno et al. separated a series of heterodinuclear DKRECPs $[\{RE(\mu_2\text{-}OH)_2RE'\}(\gamma\text{-}SiW_{10}O_{36})_2]^{10-}$ (RE = Gd^{III}, Dy^{III}; RE' = Eu^{III}, Yb^{III}, Lu^{III}) (Fig. 4b).[22] As expected, all the DyRE' species exhibit the single-molecule magnet (SMM) behavior, furthermore, their energy barriers for magnetization reversal ($\Delta E/k_B$) could be manipulated by modulating the coordination geometry and anisotropy of the Dy^{3+} ion by tuning the adjacent RE' ion in the heterodinuclear $[Dy(\mu_2\text{-}OH)_2RE']^{4+}$ moieties. The energy barriers increase in the order of DyLu ($\Delta E/k_B$ = 48 K) < DyYb (53 K) < DyDy (66 K) < DyEu (73 K) with increasing in the ionic radii of the RE' ions.[22]

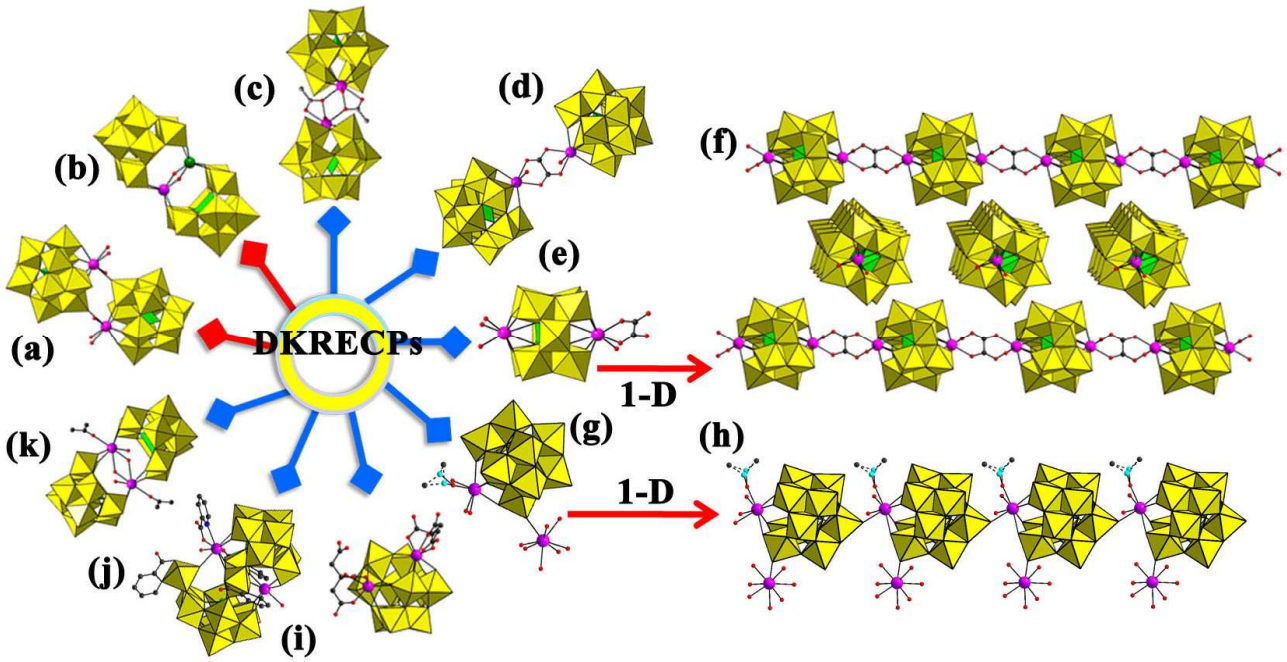

Fig. 4 (a) View of $[\{(\alpha\text{-}PW_{11}O_{39}H)RE(H_2O)_3\}_2]^{6-}$. (b) View of the heterodinuclear $[\{RE(\mu_2\text{-}OH)_2RE'\}(\gamma\text{-}SiW_{10}O_{36})_2]^{10-}$. (c) View of $[\{(\alpha\text{-}PW_{11}O_{39})RE(H_2O)(\eta^2,\mu\text{-}1,1)\text{-}CH_3COO\}_2]^{10-}$. (d) View of the oxalate-bridging $\{[(\alpha\text{-}PW_{11}O_{39})RE(H_2O)]_2(C_2O_4)\}^{10-}$. (e) View of the structural unit of $\{(\alpha\text{-x-}PW_{10}O_{38})Tm_2(C_2O_4)(H_2O)_2\}^{3-}$. (f) The interesting 1-D chain alignment of $\{(\alpha\text{-x-}PW_{10}O_{38})Tm_2(C_2O_4)(H_2O)_2\}^{3-}$. (g) View of the structural unit of $\{Sm(H_2O)_7[Sm(H_2O)_2(DMSO(\alpha\text{-}SiW_{11}O_{39})]\}^{2-}$. (h) The 1-D architecture of $\{Sm(H_2O)_7\ [Sm(H_2O)_2(DMSO(\alpha\text{-}SiW_{11}O_{39})]\}^{2-}$. (i) View of $[Tb_2(pic)(H_2O)_2(B\text{-}\beta\text{-}AsW_8O_{30})_2(WO_2(pic))_3]^{10-}$. (j) View of $[\{RE(H_2O)_2(acetone)\}_2\{\gamma\text{-}SiW_{10}O_{36}\}_2]^{10-}$. (k) View of $[Dy_2(Hcit)_2(AsW_{10}O_{38})]^{11-}$. ($WO_6$: yellow, XO_4: bright green, RE: light purple and green, O: red, S: turquiose, C: cray, N: blue).

Meanwhile, the remarkable progress on organic–inorganic hybrid DKRECPs have been made and some novel structures of this subset should be highlighted here. Niu and coworkers not only communicated a class of novel (η^2,μ-1,1)-acetato-bridging phosphotungstate-based DKRECP hybrids with discrete structures $[\{(\alpha\text{-}PW_{11}O_{39})RE(H_2O)(\eta^2,\mu\text{-}1,1)\text{-}CH_3COO\}_2]^{10-}$ (RE = Sm^{III}, Eu^{III}, Gd^{III}, Tb^{III}, Ho^{III}, Er^{III}) (Fig. 4c),[33] but also successfully obtained another two types of oxalate-bridging DKRECPs constructed by lacunary Keggin phosphotungstate-supported RE derivatives $\{[(\alpha\text{-}PW_{11}O_{39})RE(H_2O)]_2\ (C_2O_4)\}^{10-}$ (RE = Y^{III}, Dy^{III}, Ho^{III}, Er^{III}) (Fig. 4d) and $\{(\alpha\text{-}x\text{-}PW_{10}O_{38})Tm_2(C_2O_4)(H_2O)_2\}^{3-}$ (Fig. 4e).[34] It should be noted that $\{[(\alpha\text{-}PW_{11}O_{39})RE(H_2O)]_2(C_2O_4)\}^{10-}$ show the discrete structures including two mono-RE substituted Keggin $[RE(\alpha\text{-}PW_{11}O_{39})]_2^{14-}$ subunits bridged by an oxalate ligand while $[(\alpha\text{-}x\text{-}PW_{10}O_{38})Tm_2(C_2O_4)(H_2O)_2]^{3-}$ displays the 1-D chain motif formed by the unusual divacant di-Tm-containing $[\alpha\text{-}x\text{-}PW_{10}O_{38}]^{11-}$ subunits by oxalate linkers (Fig. 4f). Moreover, these interesting 1-D chains are aligned in two different spatial orientations (Fig. 4f). This construction fashion was observed for the first time in POM chemistry. In 2014, Hussain et al reported a series of (η^2,μ-1,1)-acetato-bridging silicotungstate-based DKRECP hybrids $[\{RE(\alpha\text{-}SiW_{11}O_{39})(H_2O)\}_2(\mu\text{-}CH_3COO)_2]^{12-}$ (RE = Eu^{III}, Gd^{III}, Tb^{III}, Dy^{III}, Ho^{III}, Er^{III}, Tm^{III}) by a reaction of $Na_{10}[\alpha\text{-}SiW_9O_{34}]\cdot 16H_2O$ with $RE(NO_3)_3\cdot n\ H_2O$ in KAc–HAc buffer at pH 4.5,[21b] which are almost isostructural to those phosphotungstate-based DKRECP hybrids made by Niu et al.[33] Except for the above discussed oxalate-bridging 1-D chain architecture, Niu et al also discovered another novel 1-D organic–inorganic hybrid DKRECP $\{Sm(H_2O)_7[Sm(H_2O)_2(DMSO)(\alpha\text{-}SiW_{11}O_{39})]\}^{2-}$ with mixed $[Sm(H_2O)_7]^{3+}$ and $[Sm(H_2O)_2(DMSO)]^{3+}$ pendants on both sides of the 1-D chain (DMSO = dimethyl sulfoxide) (Fig. 4g, 4h).[35] In addition, Xu et al reported a citrate-decorated Keggin-type di-Dy^{III}-containing tungstoarsenate $[Dy_2(Hcit)_2(AsW_{10}O_{38})]^{11-}$ (H_4cit = citric acid) with the two non-adjacent substituted sites occupied (Fig. 4i).[36] Notably, the citric acid ligand is first introduced to the RE–POM system and this compound is the first DKRECP with two non-adjacent substituted sites. It is well known that aromatic carboxylic acids are excellent multifunctional ligands in the construction of TMSP hybrids, therefore, they should be also able to be introduced to the system of RECPs.[37] Thus, by reaction of picH (pic = 2-picolinate), $[As_2W_{19}O_{67}(H_2O)]^{14-}$ precursor and $Tb(OAc)_3$ in the ratios of 4: 1: 2 at the acidic condition (pH 3.6–3.9), Boskovic et al separated a di-Tb^{III}-containing tungstoarsenate with pic ligands $[Tb_2(pic)(H_2O)_2(B\text{-}\beta\text{-}AsW_8O_{30})_2(WO_2(pic))_3]^{10-}$ (Fig. 4j), in which two tetra-vacant Keggin $[B\text{-}\beta\text{-}AsW_8O_{30}]^{9-}$ units oriented at 180° with respect to each other are connected by three $\{WO_2(pic)\}$ moieties and two Tb^{3+} centers.[38] Among the multitude applications of POMs, Lewis acid catalysts are very rare in comparison with the Brønsted acid and oxidation catalysts in most situations.[39,13d] Nevertheless, by virtue of the high coordination numbers and flexible coordination geometries, RE cations can not only leave residual coordination sites but also further act as effective Lewis acids for activation of substrates.[40,13c,13e] On the base of this feature, Mizuno and collaborators designed and synthesized a series of efficient POM-

based Lewis acid DKRECP catalysts $[\{RE(H_2O)_2(acetone)\}_2\{\gamma\text{-}SiW_{10}O_{36}\}_2]^{10-}$ (RE = Y^{III}, Nd^{III}, Eu^{III}, Gd^{III}, Tb^{III}, Dy^{III}) by reactions of $TBA_4H_4[\gamma\text{-}SiW_{10}O_{36}]$ with $RE(acac)_3$ in 2012 (Fig. 4k),[41] in which two silicotungstate units are pillared by two RE cations. In these DKRECP catalysts, nucleophilic oxygen-enriched surfaces of negatively charged POMs and the incorporated RE cations can respectively function as Lewis bases and Lewis acids. The experimental results of cyanosilylation of carbonyl compounds with trimethylsilyl cyanide indicate DKRECPs with larger RE cations manifest higher catalytic activities for cyanosilylation due to the higher activation ability of C=O bonds (higher Lewis acidity) and sterically less hindered Lewis acid sites. Amongst these DKRECP catalysts checked, the $[\{Nd(H_2O)_2(acetone)\}_2\{\gamma\text{-}SiW_{10}O_{36}\}_2]^{10-}$ shows the remarkable catalytic performance for cyanosilylation of various ketones and aldehydes with producing the corresponding cyanohydrin trimethylsilyl ethers in high yields.[41]

2.2.2 Dinuclear Dawson-type RECPs (DDRECPs)

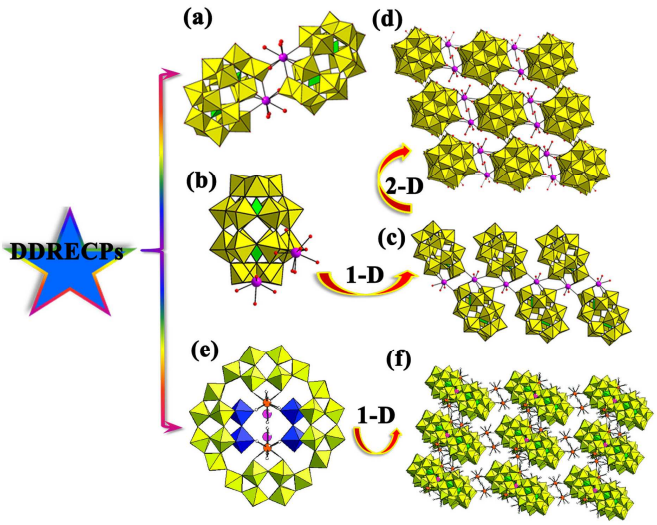

Fig. 5 (a) The centrosymmetric structure of $[\{\alpha_1\text{-}La(H_2O)_4P_2W_{17}O_{61}\}_2]^{14-}$. (b) View of the structural unit of $[Nd_2(H_2O)_9(\alpha_2\text{-}P_2W_{17}O_{61})]^{4-}$. (c) The 1-D chain motif of $[Nd(H_2O)_2(\alpha_2\text{-}P_2W_{17}O_{61})]_n^{7n-}$. (d) The 2-D extended layer of $[Nd_2(H_2O)_9(\alpha_2\text{-}P_2W_{17}O_{61})]^{4-}$. (e) View of the structural unit of $[K\subset P_8W_{48}O_{184}(H_4W_4O_{12})_2RE_2(H_2O)_{10}]^{25-}$ (Copied from ref. 42). (f) The 3-D framework of $[K\subset P_8W_{48}O_{184}(H_4W_4O_{12})_2RE_2(H_2O)_{10}]^{25-}$ (Copied from ref. 42). (WO_6: yellow and blue, XO_4: bright green, RE: light purple, O: red)

Compared with DKRECPs, the research developments of DDRECPs are laggardly and few examples have been reported during the past decade. In 2006, Hasenknopf et al separated a centrosymmetric DDRECP $[\{\alpha_1\text{-}La(H_2O)_4P_2W_{17}O_{61}\}_2]^{14-}$ in aqueous solution (Fig. 5a).[42] Such phenomenon that a RECP is composed of two monovacant Dawson phosphotungstate subunits with the α_1 configuration is very uncommon in the field of POMs. Meanwhile, by controlling the ratio of $Nd^{3+}/[\alpha_2\text{-}P_2W_{17}O_{61}]^{10-}$, Wang et al obtained the first 2-D extended structure based on $[Nd_2(H_2O)_9(\alpha_2\text{-}P_2W_{17}O_{61})]^{4-}$ DDRECP units (Fig. 5b) connected via trivalent Nd^{3+} ions under hydrothermal conditions (Fig. 5b,5c,5d).[43] In this compound, the Nd^{3+} ions located in the vacant sites of the $[\alpha_2\text{-}P_2W_{17}O_{61}]^{10-}$ fragments firstly connect adjacent $[\alpha_2\text{-}P_2W_{17}O_{61}]^{10-}$ fragments to form a 1-D chain $[Nd(H_2O)_2(\alpha_2\text{-}P_2W_{17}O_{61})]_n^{7n-}$ (Fig. 5c), and then these 1-D $[Nd(H_2O)_2(\alpha_2\text{-}P_2W_{17}O_{61})]_n^{7n-}$ chains further are combined with adjacent chains to create a 2-D extended layer by means of all Nd^{3+} ions (Fig. 5d). It should be pointed out that the most evident difference between $[\{\alpha_1\text{-}La(H_2O)_4P_2W_{17}O_{61}\}_2]^{14-}$ and $[\{Nd(H_2O)_9(\alpha_2\text{-}P_2W_{17}O_{61})\}_2]^{4-}$ is that the former comprises the monovacant $[\alpha_1\text{-}P_2W_{17}O_{61}]^{10-}$ fragments whereas the latter consists of monovacant $[\alpha_2\text{-}P_2W_{17}O_{61}]^{10-}$ fragments. As we know, the coronary $[P_8W_{48}O_{184}]^{40-}$ POA is one important derivative of Dawson POMs and can be viewed as a combination of four hexavacant Dawson $[P_2W_{12}O_{48}]^{14-}$ entities via eight W–O–W linkers. By reaction of coronary precursor $[P_8W_{48}O_{184}]^{40-}$ and early RE cations, Pope et al obtained novel 3-D frameworks constructed from $[K\subset P_8W_{48}O_{184}(H_4W_4O_{12})_2RE_2(H_2O)_{10}]^{25-}$ (RE = La^{III}, Ce^{III}, Pr^{III}, Nd^{III}) DDRECP units (Fig. 5e, 5f),[44] which opens up the study on the RE chemistry of the $[P_8W_{48}O_{184}]^{40-}$ anion.

2.2.3 Dinuclear Anderson-type RECPs (DARECPs)

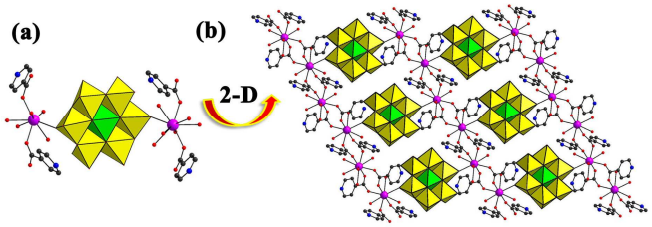

Fig. 6 (a) View of the structural unit of $[(C_6H_5NO_2)_2RE(H_2O)_4]_2[IMo_6O_{24}][NO_3]\cdot4H_2O$. (b) The 2-D extended network of $[(C_6H_5NO_2)_2RE(H_2O)_4]_2[IMo_6O_{24}][NO_3]\cdot4H_2O$. ($WO_6$: yellow, XO_4: bright green, RE: light purple, O: red, C: cray, N: blue)

During the course of probing dinuclear RECPs, the research on DARECPs remains largely unexplored because of the low surface charge of Anderson POAs. In 2004, Krebs et al obtained a family of 1-D infinite chain-like polyoxomolybdates based on DARECP building blocks $\{[La(H_2O)_6]_2(TeMo_6O_{24})\}_n\cdot6nH_2O$, $\{[Ce(H_2O)_7]_2(TeMo_6O_{24})\}_n\cdot7nH_2O$, $\{[Pr(H_2O)_7]_2(TeMo_6O_{24})\}_n\cdot8nH_2O$ and $\{[Nd(H_2O)_7]_2(TeMo_6O_{24})\}_n\cdot8nH_2O$ by reaction of telluric acid, potassium molybdate and rare earth salts in the pH 5.5 aqueous solution, however, their 1-D chain construction modes are somewhat different. In the construction of 1-D chains, the $[TeMo_6O_{24}]^{6-}$ POA acts as a hexadentate ligand for La^{3+} ions and as a tetradentate ligand for Ce^{3+}, Pr^{3+} and Nd^{3+} ions.[45a] As the extension of their work, in 2005, they found two di-RE bisupporting DARECPs $[(RE(H_2O)_6)_2(TeMo_6O_{24})]\cdot10H_2O$ (RE = Ho^{III}, Yb^{III}).[45b] These results show that the lanthanide contraction has a remarkable influence on their structural construction modes. In 2006, two unusual 2-D extended network DARECPs $[(C_6H_5NO_2)_2RE(H_2O)_4]_2[IMo_6O_{24}][NO_3]\cdot4H_2O$ (RE = La^{III}, Ce^{III}, $C_6H_5NO_2$ = pyridine-4-carboxylic acid) (Fig. 6a) were synthesized by Wang's group.[46] Interestingly, this 2-D extended network is constituted by RE coordination polymer chains

linked together by $[IMo_6O_{24}]^{5-}$ POAs (Fig. 6b) and is on behalf of the first example of 2-D inorganic–organic hybrid polyoxomolybdates based on A-type Anderson POAs.

2.2.4 Other dinuclear RECPs

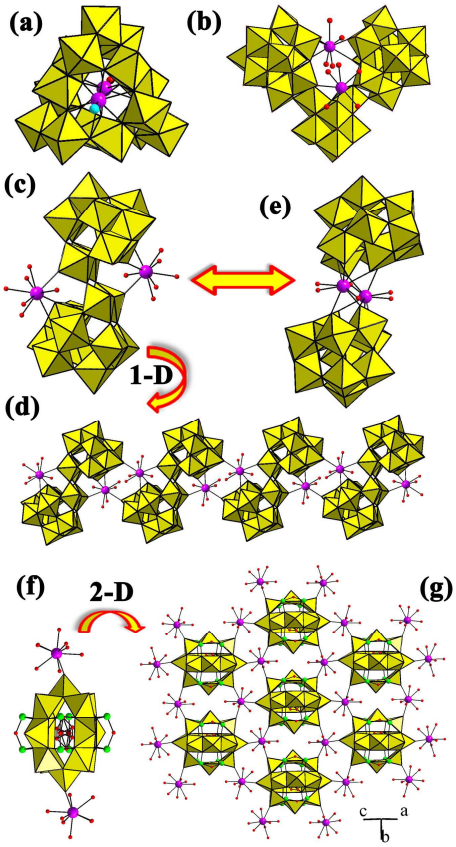

Fig. 7 (a) View of $[H_6Ce_2(H_2O)Cl(W_5O_{18})_3]^{7-}$. (b) View of $[RE_2(H_2O)_{10}W_{28}O_{93}(OH)_2]$. (c) View of the structural unit of $[RE_2(H_2O)_{10}W_{28}O_{92}(OH)_2]^{14-}$. (d) The 1-D chain fashion of $[RE_2(H_2O)_{10}W_{28}O_{92}(OH)_2]^{14-}$. (e) View of $[Ce_2(H_2O)_6W_{22}O_{72}(OH)_4]^{10-}$. (f) View of the structural unit of $[\{RE(H_2O)_6\}_2As_8V_{14}O_{42}(SO_3)]\cdot 8H_2O$. (g) The 2-D extended structure of $[\{RE(H_2O)_6\}_2As_8V_{14}O_{42}(SO_3)]\cdot 8H_2O$. ($WO_6$ and VO_5: yellow, RE: light purple, As: green, O: red, Cl: turquoise, S: dark red)

Apart from the above mentioned dinuclear RECPs, several interesting isopolymetalates stabilized by dinuclear RE cations have been also discovered in the past decade. In the field of isopolymolybdates, Evans' group reported a class of novel dinuclear RECPs based on octamolybdate units: highly hydrated $[Dy_2(H_2O)_{12}](Mo_8O_{27})\cdot 8H_2O$ and its partially dehydrated product $[Dy_2(H_2O)_6](Mo_8O_{27})$, and highly hydrated $[Nd_2(H_2O)_{12}](Mo_8O_{27})\cdot 6H_2O$ and its partially dehydrated product $[Nd_2(H_2O)_6](Mo_8O_{27})\cdot 3H_2O$,[47] and they found that the partial dehydration of both highly hydrated RE octamolybdates topotactically condenses the isolated $RE_2Mo_8O_{27}$ chains into the 3-D framework structures, leading to channels along the $[Mo_8O_{27}]^{6-}$ chain direction in the obtained products. In the domain of isopolytungstates, many building blocks have been separated such as $[W_6O_{19}]^{2-}$, $[H_4W_{11}O_{38}]^{6-}$, $[H_2W_{12}O_{40}]^{6-}$, $[H_2W_{12}O_{42}]^{10-}$, $[H_4W_{22}O_{74}]^{12-}$, and $[H_{12}W_{36}O_{120}]^{12-}$.[48] In 2006, Jiang et al synthesized a class of rare 3-D frameworks built by dinuclear RECPs $\{[RE(H_2O)_5]_2(H_2M_{12}O_{42})\}^{4-}$ (RE = La^{III}, Sm^{III}, Eu^{III}, Gd^{III}, Tb^{III}, Dy^{III}, Ho^{III}, Er^{III}, Yb^{III}, Lu^{III}; M = W or W/Mo), which are assembled from the arrangement of paradodecatungstate $[H_2M_{12}O_{42}]^{10-}$ POAs and $[RE(H_2O)_5]^{3+}$ linkers.[49] In 2008, Cao and collaborators isolated a novel dinuclear cerium(III)-containing pentadecatungstate $[H_6Ce_2(H_2O)Cl(W_5O_{18})_3]^{7-}$ with an approximate C_3 symmetry by reaction of $Na_2WO_4\cdot 2H_2O$ and $Ce(NO_3)_3\cdot 6\ H_2O$ in aqueous acidic medium (optimal pH = 5.0) (Fig. 7a).[50] The most remarkable structural characteristics of this compound is that three $[W_5O_{18}]^{6-}$ units are connected with each other to give rise to a 15-member ring by corner-sharing WO_6 octahedra and this asymmetrical 15-member ring was stabilized by two Ce^{3+} ions, in which the Cl^- ion plays a role of terminal ligand for one of the Ce^{3+} ions. Thereafter, Kortz et al synthesized the V-shaped $[RE_2(H_2O)_{10}W_{28}O_{92}(OH)_2]^{14-}$ POA (RE = Sm^{III}, Eu^{III}) by reaction of RE and WO_4^{2-} ions in aqueous acidic medium (pH = 3.2) (Fig. 7b),[51] in which the $\{W_{28}\}$ cluster is made up of two undecatungstate $\{W_{11}\}$ subunits and a hexatungstate $\{W_6\}$ subunit and one RE ion bridges two $\{W_{11}\}$ subunits together by four μ-oxo bridges while the other RE ion simultaneously coordinates to two $\{W_{11}\}$ subunits and a $\{W_6\}$ subunit by three μ-oxo bridges. In the same year, they also reported a family of *S*-shaped dinuclear RE-containing isopolytungstates $[RE_2(H_2O)_{10}W_{22}O_{72}(OH)_2]^{8-}$ (RE = La^{III}, Ce^{III}, Tb^{III}, Dy^{III}, Ho^{III}, Er^{III}, Tm^{III}, Yb^{III}, Lu^{III}) (Fig. 7c) and this *S*-shaped dinuclear RE-containing 22-isopolytungstates can be polymerized to the 1-D chain structure by the bridging role of RE ions (Fig. 7d).[52] Subsequently, Su's group also separated a novel *S*-shaped di-cerium(III) 22-isopolytungstate $[Ce_2(H_2O)_6W_{22}O_{72}(OH)_4]^{10-}$ by reaction of $Na_2WO_4\cdot 2\ H_2O$, Na_2SO_3 and $Ce(NO_3)_3\cdot 6H_2O$ (pH = 5.5), which is constructed from two discrete $\{W_{11}\}$ subunits linked through two nine-coordinate Ce^{3+} ions (Fig. 7e).[53] The obvious distinction between the above mentioned two *S*-shaped dinuclear RE-containing 22-isopolytungstates is as follows: two $[HW_{11}O_{38}]^{7-}$ subunits are directly connected with each other by sharing two oxygen atoms in $[RE_2(H_2O)_{10}W_{22}O_{72}(OH)_2]^{8-}$ whereas two $[H_2W_{11}O_{38}]^{8-}$ subunits are bridged together by two Ce^{3+} linkers in $[Ce_2(H_2O)_6W_{22}O_{72}(OH)_4]^{10-}$. In addition, utilizing the linking propensity of the sulfite encapsulated polyoxovanadate precursor $[As_8V_{14}O_{42}(SO_3)]^{6-}$ with RE cations, Das and co-workers obtained a group of novel RE-containing polyoxovanadates $[\{RE(H_2O)_6\}_2As_8V_{14}O_{42}(SO_3)]\cdot 8H_2O$ (RE = La^{III}, Sm^{III}, Ce^{III}) with 2-D extended structures.[54] In the structural unit, fourteen distorted $\{VO_5\}$ square pyramids combines with each other in the edge-sharing mode to form a $\{V_{14}\}$ cluster with a disordered SO_3^{2-} unit in the centre, and then four handle-like $\{As_2O_5\}$ units graft to the equatorial position of the $\{V_{14}\}$ cluster to construct the basic skeleton of the $[As_8V_{14}O_{42}(SO_3)]^{6-}$ cluster anion (Fig. 7f). Finally, two $[RE(H_2O)_6]^{3+}$ ions are symmetrically attached to the cluster anion by a terminal oxygen from the cluster anion. In the 2-D extended structure, each $[As_8V_{14}O_{42}(SO_3)]^{6-}$ cluster anion is surrounded by six $[RE(H_2O)_6]^{3+}$ ions whereas each $[RE(H_2O)_6]^{3+}$ ion connects with three $[As_8V_{14}O_{42}(SO_3)]^{6-}$ cluster anions (Fig. 7g).

2.3 Trinuclear RECPs

2.3.1 Trinuclear Keggin-type RECPs (TKRECPs)

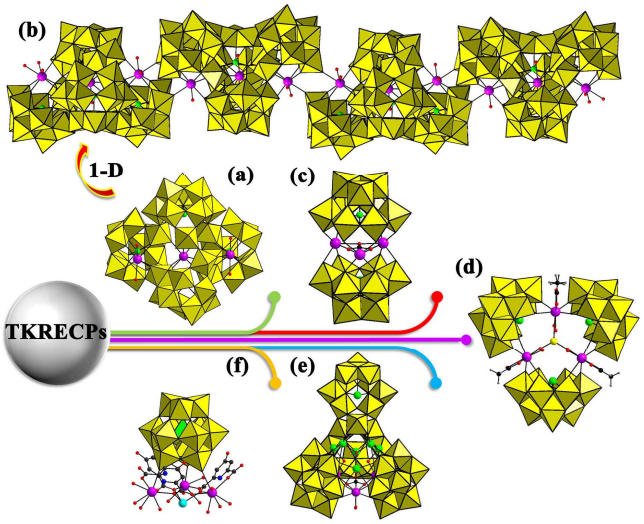

Fig. 8 (a) View of the structural unit of $[Nd_3As_4W_{41}O_{141}OH(H_2O)_{10}]^{16-}$. (b) The 1-D chain of $[Nd_3As_4W_{41}O_{141}OH(H_2O)_{10}]^{16-}$. (c) View of $[Dy_3(H_2O)_3(CO_3)(A\text{-}\alpha\text{-}AsW_9O_{34})(A\text{-}\beta\text{-}AsW_9O_{34})]^{11-}$. (d) View of $[\{Y(\alpha\text{-}SbW_9O_{31}(OH)_2)(CH_3COO)(H_2O)\}_3(WO_4)]^{17-}$. (e) View of $[(BiW_9O_{33})_4(WO_3)\{Bi_6(\mu_3\text{-}O)_4(\mu_2\text{-}OH)_3\}(RE_3(H_2O)_6CO_3)]^{22-}$. (f) View of $\{Na(H_2O)_3[RE(HCAM)(H_2O)_3]_3\}[SiW_{12}O_{40}]\cdot nH_2O$. ($WO_6$: yellow, blue and orange, X: bright green, RE: light purple, O: red, C: cray, N: blue, Na: turquiose)

Because of the existence of the lone pair electrons located on the top of trigonal pyramids of As^{III}, Sb^{III} and Bi^{III} heteroatoms, the stereochemistry effect of the lone pair electrons may act in the structural formation of POMs. Thus, As^{III}, Sb^{III} and Bi^{III} containing RECPs always exhibit unique spatial structures. Specifically speaking, the stereo-directing lone pair electrons of these heteroatoms greatly influence the further condensation of the POAs such as preventing the formation of plenary structures. Nevertheless, these lone pair electrons are beneficial to the formation of more open architectures through introducing bridging electrophiles.[55, 17a] In the past decade, many interesting trinuclear RECPs have emerged by continuous attempts of chemists. Using the adaptable precursors and the bench-top reaction condition in acidic (pH < 2) aqueous media, the 1-D chain tungstoarsenate $[Nd_3As_4W_{41}O_{141}OH(H_2O)_{10}]^{16-}$ was synthesized by Boskovic et al in 2010.[56] The $[Nd_3As_4W_{41}O_{141}OH(H_2O)_{10}]^{16-}$ POA consists of three $[B\text{-}\alpha\text{-}As^{III}W_9O_{33}]^{9-}$ and one $[B\text{-}\beta\text{-}As^{III}W_8O_{29}(OH)]^{8-}$ fragments (Fig. 8a), in which the $[B\text{-}\beta\text{-}As^{III}W_8O_{29}(OH)]^{8-}$ fragment was firstly observed. There are three crystallographically unique square antiprismatic Nd^{3+} ions in $[Nd_3As_4W_{41}O_{141}OH(H_2O)_{10}]^{16-}$ POA, moreover, a Nd^{3+} ion acts as a template for the assembly of POA and two Nd^{3+} ions work as linkers to construct the 1-D chain (Fig. 8b). Then, Xu et al reported a carbonate and trinuclear dysprosium sandwiched tungstoarsenate $K_8H_3[Dy_3(H_2O)_3(CO_3)(A\text{-}\alpha\text{-}AsW_9O_{34})(A\text{-}\beta\text{-}AsW_9O_{34})]\cdot 22H_2O$ in 2012,[41] in which three Dy^{3+} ions create an equatorial belt formed by two isomeric trivacant Keggin fragments $[A\text{-}\alpha\text{-}AsW_9O_{34}]^{9-}$ and $[A\text{-}\beta\text{-}AsW_9O_{34}]^{9-}$, and the CO_3^{2-} is encapsulated in the triangle plane (Fig. 8c), giving rise to a stable dysprosium carbonate-containing sandwich-type POM. During the exploration of novel tungstoarsenate-based TKRECPs, tungstoantimonate-based TKRECPs have also attracted increasing interest due to some similar reaction behaviors of Sb^{III} and As^{III} elements. In 2011, Kortz's group successfully synthesized a special trinuclear Y^{III}-containing tungstoantimonate $[\{Y(\alpha\text{-}SbW_9O_{31}(OH)_2)(CH_3COO)(H_2O)\}_3(WO_4)]^{17-}$ by a simple one-pot reaction of Y^{3+} ions with $[\alpha\text{-}SbW_9O_{33}]^{9-}$ and WO_4^{2-} ions in a 3:3:1 molar ratio in LiOAc/ AcOH buffer at pH 5.3 (Fig. 8d).[57] In this POA, a tetrahedral WO_4^{2-} capping unit is in the encirclement of three $[\alpha\text{-}SbW_9O_{33}]^{9-}$ units linked by three Y^{3+} ions. Although As^{III}, Sb^{III} and Bi^{III} heteroatoms all own the lone pair electrons, the ionic radius of Bi^{III} (1.17 Å) is bigger than As^{III} (0.72 Å) and Sb^{III} (0.90 Å), which renders it to exhibit a significant difference in inducing the structural diversity of RECPs. In addition, with the appearance of underlying applications in catalytic activity, ferroelectric, piezoelectric and non-linear dielectric susceptibility, tungstobismuthates are regarded as one of potential solid functional materials.[58] In 2012, Xu and coworkers isolated three unprecedented giant TKRECPs $[(BiW_9O_{33})_4(WO_3)\{Bi_6(\mu_3\text{-}O)_4(\mu_2\text{-}OH)_3\}(RE_3(H_2O)_6CO_3)]^{22-}$ (RE = Pr^{III}, Nd^{III}, La^{III}) by reacting $Na_{12}[Bi_2W_{22}O_{74}(OH)_2]\cdot 44H_2O$, $Na_9[BiW_9O_{33}]\cdot 16H_2O$ with $LnCl_3$ in the participation of Na_2CO_3 in aqueous solution (pH ~7.0) (Fig. 8e).[59] The $[(BiW_9O_{33})_4(WO_3)\{Bi_6(\mu_3\text{-}O)_4(\mu_2\text{-}OH)_3\}(RE_3(H_2O)_6CO_3)]^{22-}$ POA can be explained as follows: the $[\{Pr_3(H_2O)_6CO_3\}]^{7+}$ cation first joins three trivacant $[\alpha\text{-}B\text{-}BiW_9O_{33}]^{9-}$ fragments together forming a trigonal alignment, and then is connected to the fourth $[\alpha\text{-}B\text{-}BiW_9O_{33}]^{9-}$ fragment through a $[\{Bi_6(\mu_3\text{-}O)_4(\mu_2\text{-}OH)_3\}]^{7+}$ cation and an additional six-coordinate tungsten atom. This POA represents the largest RE-containing polyoxotungstobismuthate. Furthermore, a suitable ligand selection is the key factor to obtain the desired structural features and properties. By making use of H_3CAM (2,6-dicarboxy-4-hydroxypyridine), Mirzaei et al made a series of novel inorganic–organic hybrids $\{Na(H_2O)_3[RE(HCAM)(H_2O)_3]_3\}[SiW_{12}O_{40}]\cdot nH_2O$ (RE = La^{III}, Ce^{III}, Eu^{III}), in which a polynuclear cation $\{Na(H_2O)_3[RE(HCAM)(H_2O)_4]_3\}^{4+}$ coordinates to the $[SiW_{12}O_{40}]^{4-}$ POA (Fig. 8f).[60] Moreover, unprecedented anion–π interactions in inorganic–organic Keggin-type POM frameworks were described and analyzed for the first time.[60]

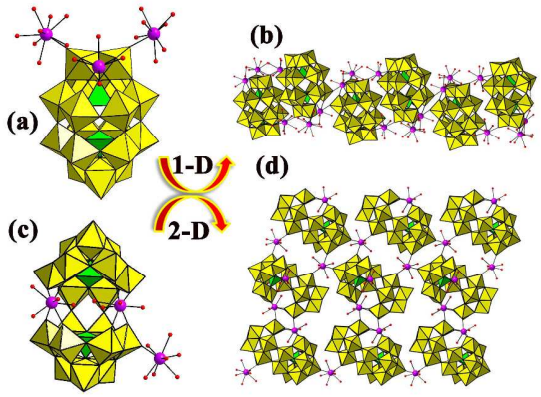

Fig. 9 (a) View of $[Nd_3(H_2O)_{17}(\alpha_2\text{-}P_2W_{17}O_{61})]^-$. (b) The 1-D chain of $[Nd_3(H_2O)_{17}(\alpha_2\text{-}P_2W_{17}O_{61})]^-$. (c) View of $Na_4Cs_3Ho[Ho_2(H_2O)_7Si_2W_{18}O_{66}]\cdot 18H_2O$. (d) The 2-D extended architecture of $Na_4Cs_3Ho[Ho_2(H_2O)_7Si_2W_{18}O_{66}]\cdot 18H_2O$. ($WO_6$: yellow, XO_4: bright green, RE: light purple, O: red)

2.3.2 Trinuclear Dawson-type RECPs (TDRECPs)

In addition to the above discussed neoteric TKRECPs, several interesting TDRECPs with infinite extended architectures were discovered. In 2006, Wang's group separated the first 1-D chain TDRECP built by monovacant Dawson anions and tri-Nd^{III} cations $[Nd_3(H_2O)_{17}(\alpha_2\text{-}P_2W_{17}O_{61})]^-$ (Fig. 9a, 9b).[43] In 2011, four open Wells–Dawson silicotungstates with similar 2-D extended structures $Na_2Cs_3H_2Tb[Tb_2(H_2O)_7Si_2W_{18}O_{66}]\cdot 17H_2O$, $Na_4Cs_3DyH[Dy_2(H_2O)_{6.5}(C_2H_4O_2)_{0.5}Si_2W_{18}O_{66}]Cl\cdot 17H_2O$, $Na_4Cs_3Ho[Ho_2(H_2O)_7Si_2W_{18}O_{66}]\cdot 18H_2O$ (Fig. 9c, 9d) and $Na_{2.5}Cs_{3.5}GdH_2[Gd_2(H_2O)_7Si_2W_{18}O_{66}](C_2H_3O_2)\cdot 16H_2O$ were isolated by Patzke et al from the one-step reaction of $Na_{10}[SiW_9O_{34}]\cdot nH_2O$ with $RE(NO_3)_3\cdot nH_2O$ in a sodium acetate buffer, which are the first open Wells–Dawson RE encapsulated silicotungstates containing $[\alpha\text{-}Si_2W_{18}O_{66}]^{16-}$ POAs.[61]

2.4 Quadrnuclear RECPs

2.4.1 Quadrnuclear Keggin-type RECPs (QKRECPs)

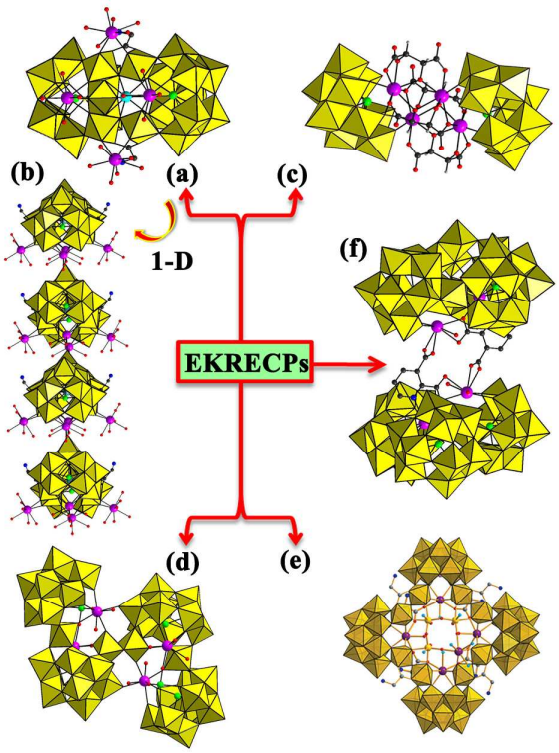

Fig. 10 (a) View of the structural unit of $[Dy_4As_2W_{22}O_{76}(H_2O)_{19}(C_2H_5NO_2)_2]^{2-}$. (b) The 1-D chain of $[Dy_4As_2W_{22}O_{76}(H_2O)_{19}(C_2H_5NO_2)_2]^{2-}$. (c) View of $[RE_2(C_4H_4O_6)(C_4H_2O_6)(AsW_9O_{33})]_2^{18-}$. (d) View of $[RE_4As_5W_{40}O_{144}(H_2O)_{10}(gly)_2]^{21-}$. (e) View of $[As^{III}_4(Y^{III}W^{VI}_3)W^{VI}_{44}Y^{III}_4O_{159}(Gly)_8(H_2O)_{14}]^{9-}$ (Copied from ref. 61). (f) View of $[As_6W_{58}O_{206}Ce_4(pydc)_2)(H_2O)_6]^{38-}$. ($WO_6$: yellow, blue and orange, RE: light purple, Na: turquiose, O: red, C: cray, N: blue)

In the preparations of QKRECPs, the divacant $[As_2W_{19}O_{67}(H_2O)]^{14-}$ precursor has aroused considerable interest and stimulated the production of a class of novel $\{AsW_9O_{33}\}$-based QKRECPs because of the following reasons: (i) the stereo-directing influence of the lone pair on the As^{III} atom allows the formation of lacunary Keggin fragments and endows the distinctive reactivity compared with those defect POM moieties anchoring tetrahedral heteroatom groups;[2] (ii) the $\{WO(H_2O)\}$ linker between two $[B\text{-}\alpha\text{-}AsW_9O_{33}]^{9-}$ fragments could serve as a starting point for rotation and dissociation, which may facilitate the generation of various building blocks in solution at different pH values;[37] (iii) This precursor is easier to be prepared in good yield. In the following discussion, the statements will be expanded according to the number of $\{AsW_9O_{33}\}$ subunits per compound. Utilizing the preformed precursor and disassembly and reassembly processes, Boskovic et al obtained a novel QKRECP $[Dy_4As_2W_{22}O_{76}(H_2O)_{19}(C_2H_5NO_2)_2]^{2-}$ ($C_2H_5NO_2$ = glycine) involving two glycine ligands (Fig. 10a).[56] This skeleton of the $[Dy_4As_2W_{22}O_{76}(H_2O)_{19}(C_2H_5NO_2)_2]^{2-}$ POA is assembled from two $[B\text{-}\alpha\text{-}AsW_9O_{33}]^{9-}$ fragments connected via two unprecedented $\{W_2O_5(glycine)\}$ groups accompanying each glycine ligand coordinating to two W^{VI} centers in a bidentate fashion. Moreover, in this compound, the Dy^{3+} cations act as linkers to form the novel 1-D chain architecture (Fig. 10b). Very recently, Niu et al obtained six tartrate-bridging tetra-RE substituted QKRECP dimers $[RE_2(C_4H_4O_6)(C_4H_2O_6)(AsW_9O_{33})]_2^{18-}$ (RE = Ho^{III}, Er^{III}, Tm^{III}, Yb^{III}, Lu^{III}, Y^{III}) (Fig. 10c),[62] which consists of two $[B\text{-}\alpha\text{-}AsW_9O_{33}]^{9-}$ fragments in a stagger fashion, sandwiching a unique cage-like RE–organic cluster formed by four RE cations and four tartaric acid segments. Three more kinds of novel QKRECPs containing four $[AsW_9O_{33}]^{9-}$ fragments have been synthesized by the precursor $[As_2W_{19}O_{67}(H_2O)]^{14-}$ in the past decade. For example, in 2011, Boskovic and collaborators synthesized and characterized a new family of QKRECPs with gly ligands $[RE_4As_5W_{40}O_{144}(H_2O)_{10}(gly)_2]^{21-}$ (RE = Gd^{III}, Tb^{III}, Dy^{III}, Ho^{III}, Y^{III}), in which two $[As_2W_{19}O_{68}]^{16-}$ subunits are bridged together by four RE cations and two tungsten centers (Fig. 10d).[63] In the formation of this series of compounds, the $[As_2W_{19}O_{67}(H_2O)]^{14-}$ POA experiences a structural rearrangement so as to accommodate inclusion of the RE ions, with transformation into the $[As_2W_{19}O_{68}]^{16-}$ subunits. This process occurs via loss of the terminal aqua ligand from the $\{WO_5(H_2O)\}$ linker, with the subsequent change .in the respective orientation of two trivacant $[B\text{-}\alpha\text{-}AsW_9O_{33}]^{9-}$ fragments. Alternating current magnetic susceptibility data have indicated the onset of slow magnetic relaxation for $[Dy_4As_5W_{40}O_{144}(H_2O)_{10}(gly)_2]^{21-}$ with the energy barrier to magnetization reversal determined to be 3.9(1) K. Furthermore, its X-band EPR spectrum further shows the presence of a non-negligible fourth order transverse component of the anisotropy, which is responsible for the small effective energy barrier observed for $[Dy_4As_5W_{40}O_{144}(H_2O)_{10}(gly)_2]^{21-}$. To date, it represents the first POM-supported polynuclear lanthanoid-based SMM.[63] In 2014, Boskovic's group first afforded a novel QKRECP $[As_4(YW_3)W_{44}Y_4O_{159}(Gly)_8(H_2O)_{14}]^{9-}$ (Fig. 10e) by incorporation of glycine (Gly) ligands into an yttrium-tungstoarsenate structural backbone and then utilized the site-selective incorporation of Mo and replacement of glycine with enantiopure L- or D-norleucine (L- or D-Nle) giving rise to two enantiomorphic compounds $\{[As^{III}_4(Mo^V_2Mo^{VI}_2)W^{VI}_{44}Y^{III}_4O_{160}(L\text{-}Nle)_9(H_2O)_{11}]\}^{18-}$ and $[As^{III}_4(Mo^{VI}_2W^{VI}_2)W^{VI}_{44}Y^{III}_4O_{160}(D\text{-}Nle)_9(H_2O)_{11}]\}^{18-}$.[64] They all consist of four $[B\text{-}\alpha\text{-}AsW_9O_{33}]^{9-}$ fragments bridged by a cyclic $\{Y_4W_8L_8\}$ (L= zwitterionic Gly, L-Nle, D-Nle) unit. Nevertheless, by means of the intensive structural, spectroscopic, electrochemical, magnetochemical and theoretical investigation, the site-selective metal substitution and photoreduction capability of the tetranuclear $\{M_4O_4\}$ core of these hybrid POAs were also elucidated.[64] In 2014, Niu et al synthesized a unique large Ce-containing POM–carboxylate hybrid $[As_6W_{58}O_{206}Ce_4$

$(pydc)_2)H_2O)_6]^{38-}$ (H_2pydc = pyridine-2,3-dicarboxylic acid) containing six $[B\text{-}\alpha\text{-}AsW_9O_{33}]^{9-}$ subsets by the bridging role of two pydc ligands (Fig. 10f).[65] It shouldn't be neglected that the trivacant precursor $[B\text{-}\alpha\text{-}AsW_9O_{33}]^{9-}$ can also construct some novel QKRECPs due to the excellent coordination ability of the vacant sites. Thereby, Wang et al successfully synthesized three large Ce-containing tungstoarsenate aggregates $[\{Ce_2O(H_2O)_5\}\{WO(H_2O)\}\{AsW_9O_{33}\}_2]_2^{16-}$, $[Ce_4As_4W_{41}O_{149}]^{24-}$ and $[Ce_4As_4W_{44}O_{151}(ala)_4(OH)_2(H_2O)_{10}]^{12-}$ (ala = L-α-alanine) by the precursor $[B\text{-}\alpha\text{-}AsW_9O_{33}]^{9-}$ using via a step-by-step assembly process.[66a] The tetrmeric POA $[\{Ce_2O(H_2O)_5\}\{WO(H_2O)\}\{AsW_9O_{33}\}_2]_2^{16-}$ is constructed from two sandwich-type $[\{Ce_2O(H_2O)_5\}\{WO(H_2O)\}\{AsW_9O_{33}\}_2]^{8-}$ moieties bridged by two Ce^{4+} ions (Fig. 11a). In the POA $[Ce_4As_4W_{41}O_{149}]^{24-}$, four Ce^{4+} ions function as linkers to link four $[B\text{-}\alpha\text{-}AsW_9O_{33}]^{9-}$ units, generating a new type of cryptand cluster (Fig. 11b). In contrast to the classical cryptate POA $[As_4W_{40}O_{140}]^{28-}$,[66b, c] $[Ce_4As_4W_{41}O_{149}]^{24-}$ can be considered that the positions of four W linkers are replaced by four Ce^{4+} centers. The unusual alanine-decorated cryptand-type POA $[Ce_4As_4W_{44}O_{151}(ala)_4(OH)_2(H_2O)_{10}]^{12-}$ is assembled from four $[B\text{-}\alpha\text{-}AsW_9O_{33}]^{9-}$ subunits connected by two $\{WO_2\}$, two $\{W_2O_5(ala)\}$, two $\{Ce_2(H_2O)_5(ala)\}$ and a linear $\{W_2O_5(OH)_2\}$ group (Fig. 11c), in which four organic α-alanine ligands are coordinated directly on the surface of the aggregate. Apart from $\{AsW_9O_{33}\}$-based QKRECPs, other QKRECPs were also discovered. For instance, two QKRECPs $[RE_4(\alpha(1,4)\text{-}GeW_{10}O_{38})_2(H_2O)_6]^{12-}$ (RE = Dy^{III}, Er^{III}) containing two $[\alpha(1,4)\text{-}GeW_{10}O_{38}]^{12-}$ subunits were made by Xu et al based on the $[\gamma\text{-}GeW_{10}O_{36}]^{8-}$ precursor, which represent the first RECP with two dilacunary Keggin-type POA units sandwiching four RE ions (Fig. 12a).[67] Different from the Xu's method, Reinoso et al utilized GeO_2, Na_2WO_4 and RE cations in NaOAc buffer to obtain a series of QKRECPs $[RE_4(H_2O)_6(\beta\text{-}GeW_{10}O_{38})_2]^{12-}$ (RE = Gd^{III}, Tb^{III}, Dy^{III}, Ho^{III}, Er^{III}, Tm^{III}, Yb^{III}, Lu^{III}).[68] In addition, Niu and coworkers reported an interesting double-parallel chain germanotungstate based on QKRECP subunits $\{[Sm_2(GeW_{11}O_{39})(DMSO)_3(H_2O)_6]\}_2^{4-}$ (Fig. 12b),[20d] in which the two parallel chains $\{[Sm(GeW_{11}O_{39})(DMSO)(H_2O)_2]^{5-}\}_n$ are joined together through $[Sm(DMSO)_2(H_2O)_4]^{3+}$ moieties (Fig. 12c). Other else, Liu et al reported a tri-Nb^V substituted germanotungstate-based QKRECP $[(GeW_9Nb_3O_{40})_4Eu_4(H_2O)_{22}]^{16-}$ (Fig. 12d),[69] which is made up of four tri-Nb^V substituted Keggin $[GeW_9Nb_3O_{40}]^{7-}$ segments bond by four Eu^{3+} cations. In addition, Wang et al communicated a tungstoantimonate-based QKRECP $[\{Y(H_2O)_7\}_4Sb_2W_{22}O_{76}]^{2-}$, in which a Krebs-type $[Sb_2W_{22}O_{76}]^{14-}$ subunit was supported by four Y^{3+} ions.[70]

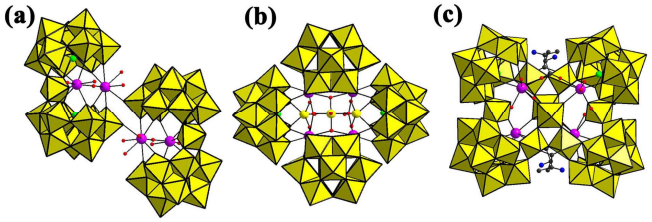

Fig. 11 (a) View of $[\{Ce_2O(H_2O)_5\}\{WO(H_2O)\}\{AsW_9O_{33}\}_2]_2^{16-}$. (b) View of $[Ce_4As_4W_{41}O_{149}]^{24-}$. (c) View of $[Ce_4As_4W_{44}O_{151}(ala)_4(OH)_2(H_2O)_{10}]^{12-}$. ($WO_6$: yellow, XO_4: bright green, RE: light purple, O: red, C: cray, N: blue)

2.4.2 Quadrnuclear Dawson-type RECPs (QDRECPs)

Through the one-step reaction of $Na_{10}[SiW_9O_{34}]_3\cdot nH_2O$ with $Gd(NO_3)_3\cdot nH_2O$ in a sodium acetate buffer, Patzke et al synthesized a novel QDRECP $\{Gd_2(H_2O)_{13}[Gd_2(H_2O)_7Si_2W_{18}O_{66}]\}^{4-}$ (Fig. 13a),[61] in which two Gd^{3+} cations are located in the peripheral pocket of the $[\alpha\text{-}Si_2W_{18}O_{66}]^{16-}$ anion whereas two Gd^{3+} cations are bound to the terminal oxygen atoms of both sides. More intriguingly, adjacent $[Gd_2(H_2O)_7Si_2W_{18}O_{66}]^{10-}$ moieties are combined together through the Gd^{3+} cations located on both sides forming the 3-D framework, represents the first 3D inorganic coordination polymer based on Ln-substituted Wells–Dawson POMs. In 2005, Hill et al separated a novel sandwich-type QDRECP

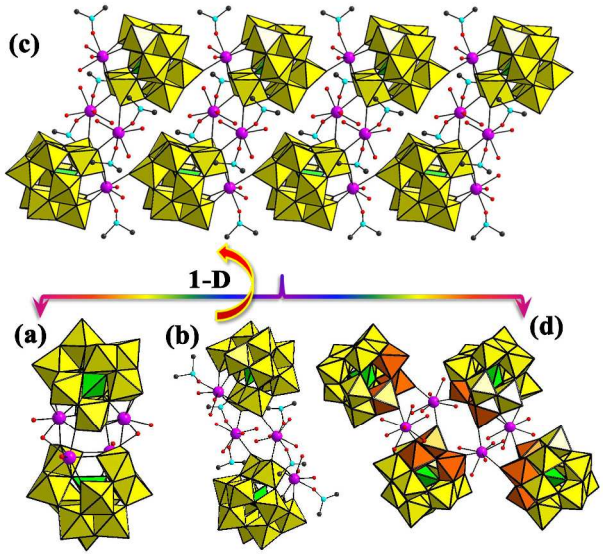

Fig. 12 (a) View of $[RE_4(\alpha(1,4)\text{-}GeW_{10}O_{38})_2(H_2O)_6]^{12-}$. (b) View of the structural unit of $\{[Sm_2(GeW_{11}O_{39})(DMSO)_3(H_2O)_6]\}_2^{4-}$. (c) View of the 1-D chain of $\{[Sm_2(GeW_{11}O_{39})(DMSO)_3(H_2O)_6]\}_2^{4-}$. (d) View of $[(GeW_9Nb_3O_{40})_4Eu_4(H_2O)_{22}]^{16-}$. ($WO_6$: yellow, NbO_6: orange, XO_4: bright green, RE: light purple, O: red, S: turquiose, C: cray, N: blue)

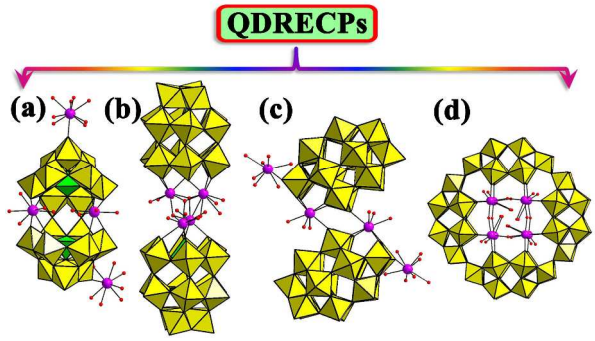

Fig. 13 (a) View of $\{Gd_2(H_2O)_{13}[Gd_2(H_2O)_7Si_2W_{18}O_{66}]\}^{4-}$. (b) View of $[\{Y_4(\mu_3\text{-}OH)_4(H_2O)_8\}(\alpha\text{-}P_2W_{15}O_{56})_2]^{16-}$. (c) View of $\{[Nd(H_2O)_7]_2[Nd(H_2O)_3(\alpha_2\text{-}P_2W_{17}O_{61})]_2\}^{8-}$. (d) View of $\{[RE_2(\mu\text{-}OH)_4(H_2O)_{12}]_2(H_{24}P_8W_{48}O_{184})\}^{12-}$. ($WO_6$: yellow, XO_4: bright green, RE: light purple, O: red)

$[\{Y_4(\mu_3\text{-}OH)_4(H_2O)_8\}(\alpha\text{-}P_2W_{15}O_{56})_2]^{16-}$ consisting of a $\{Y_4(OH)_4\}$ cubane cluster encapsulated by two trivacant Dawson $[\alpha\text{-}P_2W_{15}O_{56}]^{12-}$ subunits (Fig. 13b).[71] In the same year, a fascinating bisupporting DDRECP $\{[Nd(H_2O)_8]_2[Nd(H_2O)_3(\alpha_2\text{-}P_2W_{17}O_{61})]_2\}^{8-}$ (Fig. 13c) was found by Wang et al, which is assembled from a dimeric $[\{Nd(H_2O)_3(\alpha_2\text{-}P_2W_{17}O_{61})\}_2]^{14-}$ anion and two $[Nd(H_2O)_7]^{3+}$ cations.[43] The dimeric $[\{Nd(H_2O)_3(\alpha_2\text{-}P_2W_{17}O_{61})\}_2]^{14-}$ anion is made up of two $[P_2W_{17}O_{61}Nd(H_2O)_3]^{7-}$ subunits connected via two common terminal oxygen atoms. In 2013, Yang et al reported the $\{P_8W_{48}\}$ including QDRECPs $\{[RE_2(\mu\text{-}OH)_4(H_2O)_{12}]_2(H_{24}P_8W_{48}O_{184})\}^{12-}$ [RE = Sm^{III}, Tb^{III}] (Fig. 13d),[72] in which each Sm^{3+} ion in the cavity is positionally disordered and has a site occupancy of 0.5.

2.4.3 Quadrnuclear Lindqvist-type RECPs (QLRECPs)

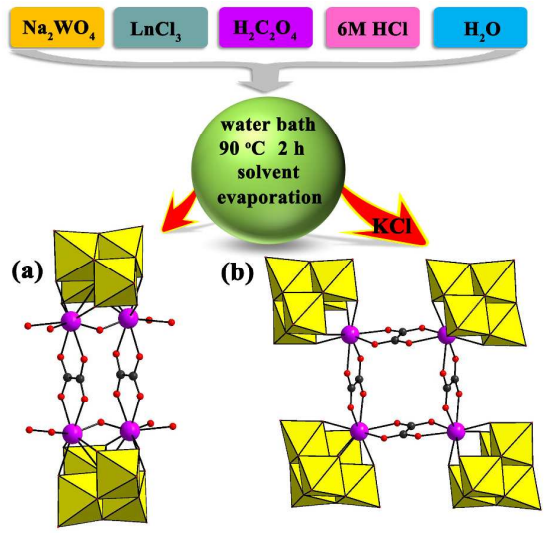

Fig. 14 (a) View of $[RE_2(C_2O_4)(H_2O)_4(OH)W_4O_{16}]_2^{10-}$. (b) View of $[RE(C_2O_4)W_5O_{18}]_4^{20-}$. ($WO_6$: yellow, RE: light purple, O: red, C: cray)

In 2014, our group made a groundbreaking work in the development of QLRECPs and successfully obtained two types of unique oxalate-connective QLRECPs $[RE_2(C_2O_4)(H_2O)_4(OH)W_4O_{16}]_2^{10-}$ (Fig. 14a) and $[RE(C_2O_4)W_5O_{18}]_4^{20-}$ (RE = Eu^{III}, Ho^{III}, Er^{III}, Tb^{III}) (Fig. 14b).[73] It should be pointed out that $[RE_2(C_2O_4)(H_2O)_4(OH)W_4O_{16}]_2^{10-}$ were obtained when only Na^+ ions are present in the reaction, whereas $[RE(C_2O_4)W_5O_{18}]_4^{20-}$ were formed when Na^+ and K^+ ions are used in the reaction. $[RE_2(C_2O_4)(H_2O)_4(OH)W_4O_{16}]_2^{10-}$ stand for the first rectangular double-oxalate-bridging tetra-Ln cluster encapsulated divacant Lindqvist isopolyoxotungstate hybrids and $[RE(C_2O_4)W_5O_{18}]_4^{20-}$ represent the first square double-oxalate-bridging tetra-Ln cluster anchored isopolyoxotungstate hybrids. This work provides the remarkable feasibility for constructing unprecedented gigantic hybrid poly(isopolyoxotungstate) species with special properties. Moreover, the solid-state luminescent and decay behavior of $[RE_2(C_2O_4)(H_2O)_4(OH)W_4O_{16}]_2^{10-}$ and $[RE(C_2O_4)W_5O_{18}]_4^{20-}$ (RE = Eu^{III}, Tb^{III}) have been profoundly probed.[73] Moreover, Niu and coworkers reported the first class of novel tetranuclear RE-containing peroxopolyoxotungstate $[RE_4(WO_4)(H_2O)_{16}\{W_7O_{22}(O_2)_2\}_4]^{14-}$ (RE = La^{III}, Pr^{III}) with a WO_4^{2-} template core (Fig. 15a).[74] The central WO_4^{2-} core and four tetradentate building blocks $\{W_7O_{22}(O_2)_2\}$ are bridged together by four $\{REO_9\}$ linkers with distorted tricapped trigonal prism coordination geometry, moreover, the central WO_4^{2-} core exhibits an interesting tetrahedral geometry. Seven W atoms are regularly arranged in the bent 2–3–2 pattern to finish the skeleton of $\{W_7O_{22}(O_2)_2\}$, in which two W atoms in the opposite sides of $\{W_3\}$ hinge exhibit distorted pentagonal bipyramidal coordination environment and the remaining W atoms adopt the common WO_6 octahedral geometry (Fig. 15b). In 2014, Su's group explored a versatile one-pot strategy to obtain two tetra-Ce^{III} containing polyoxotungstate nanoclusters $[Ce_4(H_2O)_{12}W_{44}O_{144}(OH)_{12}]^{24-}$ (Fig. 15c) (pH = 4.5) and $[Ce_2(H_2O)_9W_{36}O_{110}(OH)_{12}]_2^{20-}$ (Fig. 15e) (pH = 1.5), which represent the largest RE-containing isopolyoxotungstates to date.[53] The former is a tetrameric POA based on four novel $\{CeW_{11}\}$ building blocks linked by four Ce^{3+} bridges, in which the $\{W_{11}\}$ fragment (Fig. 15d) is derived from the α-Keggin $[H_2W_{12}O_{40}]^{6-}$ by removal of a $\{WO_6\}$ octahedron. The latter is a dimeric POA containing two identical $\{Ce_2W_{36}\}$ subunits related by an inversion center. In $\{Ce_2W_{36}\}$ subunit, one Ce^{3+} cation is trapped at the bottom of the central cavity in $\{W_{36}\}$ entity and the other Ce^{3+} cation attaches to the flank of the $\{W_{36}\}$ entity. The two $\{W_{36}\}$ entities are combined by two "attached" Ce^{3+} cations and stabilized by two "trapped" Ce^{3+} cations. The $\{W_{36}\}$ entity is constructed from three $\{W_{11}\}$ fragments (Fig. 15f) linked by three $\{WO_6\}$ octahedra. it is worthy to mention that the $\{W_{11}\}$ fragment (Fig. 15f) in the latter is completely distinct from he $\{W_{11}\}$ fragment (Fig. 15d) in the former.

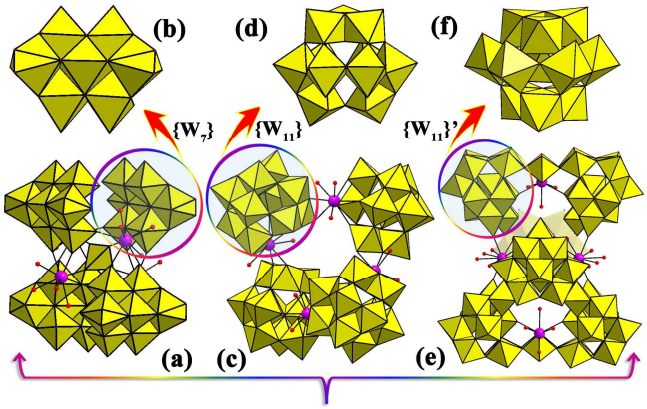

Fig. 15 (a) View of $[RE_4(H_2O)_{16}(MoO_4)\{Mo_7O_{22}(O_2)_2\}_4]^{14-}$. (b) The $\{W_7O_{22}(O_2)_2\}$ fragment in $[RE_4(H_2O)_{16}(MoO_4)\{Mo_7O_{22}(O_2)_2\}_4]^{14-}$. (c) View of $[Ce_4(H_2O)_{12}W_{44}O_{144}(OH)_{12}]^{24-}$. (d) The $\{W_{11}\}$ fragment in $[Ce_4(H_2O)_{12}W_{44}O_{144}(OH)_{12}]^{24-}$. (e) View of $[Ce_2(H_2O)_9W_{36}O_{110}(OH)_{12}]_2^{20-}$. (f) The $\{W_{11}\}$ fragment in $[Ce_2(H_2O)_9W_{36}O_{110}(OH)_{12}]_2^{20-}$. To show structures more clearly, some polyhedra are faded. (WO_6: yellow, orange, RE: light purple, O: red)

2.5 Pentanuclear Keggin-type RECPs (PKRECPs)

In the past ten years, only several PKRECPs were reported. In 2006, Krebs et al separated an unique PKRECP $[Ho_5(H_2O)_{16}(OH)_2As_6W_{64}O_{220}]^{25-}$ (Fig. 16a) consisting of six trivacant Keggin $[B\text{-}\alpha\text{-}AsW_9O_{33}]^{9-}$ subunits joined by a bridging $[Ho_5W_{10}(H_2O)_{16}(OH)_2O_{22}]^{29-}$ group, which exhibits an neoteric arrangement fashion of six trilacunary Keggin $[B\text{-}\alpha\text{-}AsW_9O_{33}]^{9-}$ subunits.[75] In 2010–2012, An and coworkers discovered several 3-D extended inorganic frameworks based on PKRECP units $[REK(H_2O)_{12}][RE(H_2O)_6]_2[(H_2O)_4REBW_{11}O_{39}H]_2\cdot 20H_2O$ (RE = Ce^{III},

Nd^{III}) (Fig. 16b), $\{RE[(H_2O)_6RE]_2[(H_2O)_4RESiW_{11}O_{39}]_2\}^-$ (RE = La^{III}, Ce^{III}) and $\{[(H_2O)_6Nd]_2[(H_2O)_7Nd][(H_2O)_4NdSiW_{11}O_{39}][(H_2O)_3NdSiW_{11}O_{39}]\}^-$.[76] Notably, $[RE(H_2O)_{12}][RE(H_2O)_6]_2[(H_2O)_4REBW_{11}O_{39}H]_2\cdot 20H_2O$ is made up of RE-substituted double Keggin-type POAs $[\{(H_2O)_4RE(BW_{11}O_{39}H)\}_2]^{10-}$ linked by Ln cations to generate a 3-D open framework with 1-D channels (Fig. 16c), $\{RE[(H_2O)_6RE]_2[(H_2O)_4RESiW_{11}O_{39}]_2\}^-$ demonstrates the similar 3-D open framework with 1-D channels to $[RE(H_2O)_{12}][RE(H_2O)_6]_2[(H_2O)_4REBW_{11}O_{39}H]_2\cdot 20H_2O$, and $\{[(H_2O)_6Nd]_2[(H_2O)_7Nd][(H_2O)_4NdSiW_{11}O_{39}][(H_2O)_3NdSiW_{11}O_{39}]\}^-$ reveals the other 3-D open framework constructed from two kinds of building blocks $[\{(H_2O)_4Nd(SiW_{11}O_{39})\}_2]^{10-}$ and $[\{(H_2O)_3Nd(SiW_{11}O_{39})\}_2]^{10-}$ that are concatenated together by Nd^{3+} cations. In 2012, a neoteric W/Nb mixed-addendum quadrangular PKRECP $[Cs(GeW_9Nb_3O_{40})_4(SO_4)Eu_5(H_2O)_{36}]^{14-}$ (Fig. 16d) was isolated by Liu's group, which is composed of two telephone-receiver-like $\{(GeW_9Nb_3O_{40})_2Eu_2\}$ (Fig. 16e) building units linked by two Eu^{3+} cations via O–Eu–O bridges. It should be pointed out that one of the Eu^{3+} cations in a telephone-receiver-like building unit is substituted by an eleven-coordinate Cs^+ cation and a sulfate ion bridges the Cs^+ ion and an adjacent Eu^{3+} ion leading to the symmetry of the quadrangle decreasing from D_{2h} to C_s.[69] In addition, Niu et al prepared a novel 1-D chain-like $\{La_6\}$ containing peroxoisopolyoxomolybdate $[H_4La_5(H_2O)_{21}(MoO_4)\{Mo_7O_{22}(O_2)_2\}_4]^{7-}$ (Fig. 17b), in which adjacent tetra-La^{III} including peroxopolyoxomolybdate $[La_4(MoO_4)(H_2O)_{16}\{Mo_7O_{22}(O_2)_2\}_4]^{14-}$ (Fig. 17a) units are connected by additional La^{3+} cations to create the 1-D structure.[77]

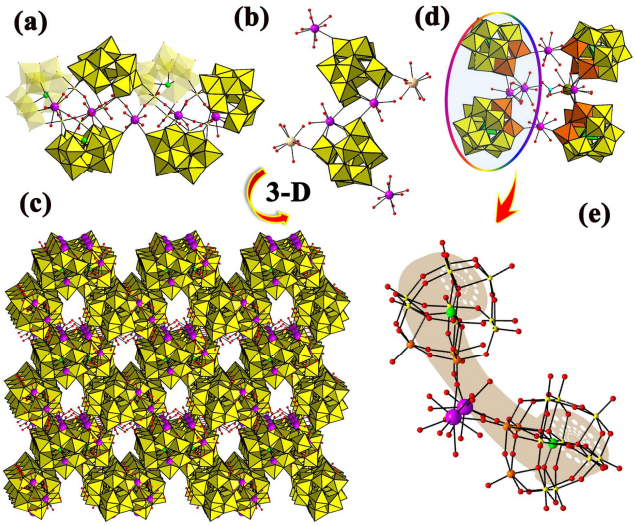

Fig. 16 (a) View of $[Ho_5(H_2O)_{16}(OH)_2As_6W_{64}O_{220}]^{25-}$. (b) View of $[REK(H_2O)_{12}][RE(H_2O)_6]_2[(H_2O)_4REBW_{11}O_{39}H]_2\cdot 20H_2O$. (c) The 3-D extended framework of $[REK(H_2O)_{12}][RE(H_2O)_6]_2[(H_2O)_4REBW_{11}O_{39}H]_2\cdot 20H_2O$ showing 1-D channels. (d) View of $[Cs(GeW_9Nb_3O_{40})_4(SO_4)Eu_5(H_2O)_{36}]^{14-}$. (e) The telephone receiver-like building unit in $[Cs(GeW_9Nb_3O_{40})_4(SO_4)Eu_5(H_2O)_{36}]^{14-}$. To show structures more clearly, some polyhedra are faded. (WO_6: yellow, NbO_6: orange, XO_4: bright green, RE: light purple, O: red, Cs: dark yellow, S: turquoise)

2.6 Hexanuclear RECPs

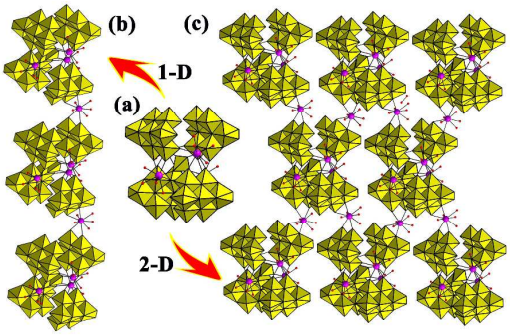

Fig. 17 (a) View of the tetra-Ln including peroxopolyoxomolybdate $[RE_4(MoO_4)(H_2O)_{16}\{Mo_7O_{22}(O_2)_2\}_4]^{14-}$. (b) The 1-D chainlike structure of $[H_4La_5(H_2O)_{21}(MoO_4)\{Mo_7O_{22}(O_2)_2\}_4]^{7-}$. (c) The 2-D extended architecture $[H_3RE_6(H_2O)_{26}(MoO_4)\{Mo_7O_{22}(O_2)_2\}_4]^{7-}$. ($WO_6$: yellow, bright green, RE: light purple, O: red)

In 2008, Boskovic and collaborators communicated a $\{Gd_6\}$ incorporated hexanuclear Keggin RECP (HKRECP) with additional acetate ligands $[Gd_6As_6W_{65}O_{229}(OH)_4(H_2O)_{12}(OAc)_2]^{38-}$ (Fig. 18a) that comprises four $[B\text{-}\alpha\text{-}AsW_9O_{33}]^{9-}$ and two $[B\text{-}\beta\text{-}AsW_9O_{33}]^{9-}$ trivacant Keggin subunits that are connected together through corner sharing with an edge-shared $\{W_3O_{13}\}$ group, two edge-shared $\{W_2O_{10}\}$ groups and four $\{WO_6\}$ octahedral,[17a] which represents the highest nuclearity POM-encapsulated Gd^{III} complex. Its variable temperature magnetic susceptibility investigation reveals spin-only magnetism with a near perfect Curie-type temperature dependence of the susceptibility.[17a] Furthermore, some extended architectures including HKRECP building units were also discovered. For instance, Li et al obtained a series of 1-D chain-like QKRECPs $[RE_6(H_2O)_x\{As_4W_{44}(OH)_2(proline)_2O_{151}\}]^{10-}$ (Fig. 18b) (RE = Tb^{III}, Dy^{III}, x = 22; RE = Nd^{III}, x = 26) in 2013,[78] and adjacent $[RE_6(H_2O)_x\{As_4W_{44}(OH)_2(proline)_2O_{151}\}]^{10-}$ clusters are linked together by double eight-coordinate RE cations producing the1-D chain motif (Fig. 18c). It is worth mentioning that the $[RE_6(H_2O)_x\{As_4W_{44}(OH)_2(proline)_2O_{151}\}]^{10-}$ cluster consists of four $[B\text{-}\alpha\text{-}AsW_9O_{33}]^{9-}$ fragments, two $\{WO_2\}$ fragments, two unfamiliar $\{W_2O_5(proline)\}$ moieties, one $\{W_2O_5(OH)_2\}$ dimer and four hydrated $\{RE(H_2O)_n\}$ (n = 2 or 3) ions. Niu and coworkers also reported a type of novel 3-D extended architecture with hybrid HKRECP units $[RE(HL)(L)(H_2O)_6\{RE(H_2L)_{0.5}(\alpha\text{-}PW_{11}O_{39}H)RE(H_2O)_4\}]_2$ (RE = La^{III}, Ce^{III}, H_2L = 2,5-pyridinedicarboxylic acid) (Fig. 18d, 18e) and examined their photocatalysis properties for degradation of rhodamine-B (RhB) upon 500 W Hg lamp irradiation.[79] Liu's group reported a 1-D Nb/W mixed-addendum HKRECP $[(GeW_9Nb_3O_{40})_4Eu_{5.5}(H_2O)_{26}]^{11.5-}$ (Fig. 18f, 18g) assembled from telephone receiver-like $\{(GeW_9Nb_3O_{40})_2Eu_2\}$ building units by sharing water ligands from adjacent Eu^{3+} cations,[69] and two isostructural hexanuclear Dawson-type RECPs (HDRECPs) with formula unit of $[RE_6(H_2O)_{38}(P_2W_{15}Nb_3O_{62})_4]^{18-}$ (RE = Eu^{III}, Ce^{III}) (Fig. 18h) and its 1-D chain alignment is constructed from sandwich-type tri-Nb^V substituted Dawson $[RE_3(P_2W_{15}Nb_3O_{62})_2]^{9-}$ fragments linked by alternative RE–O–W bridges (Fig. 18i).[80] Reviewing the history, in 2005 Hill et al synthesized a sandwich POM-supported hydroxo/oxo cluster $[\{Yb_6(\mu_6\text{-}O)(\mu_3\text{-}OH)_6(H_2O)_6\}(\alpha\text{-}P_2W_{15}O_{56})_2]^{14-}$ anchoring a trigonal antiprismatic hexa-Yb^{III} cluster around a μ_6-oxo atom, which was obtained from the carbonate-assisted hydrolysis of Yb^{3+} cations in the participation of the trivacant Dawson $[\alpha\text{-}P_2W_{15}O_{56}]^{12-}$ precursor (Fig.

18j).[71] Its magnetization measurements reveal the existence of intermolecular dipolar exchange interactions below 15 K.[71] In 2013, Niu et al reported an unprecedented HDRECP hexamer $\{Na_{12}[(\alpha_2\text{-}P_2W_{17}O_{61}H_2)La(H_2O)_4]_6\}^{6-}$ (Fig. 18k) established by two trimeric $[(\alpha_2\text{-}P_2W_{17}O_{61}H_4)La(H_2O)_4]_3^{9-}$ subunits linked by twelve Na^+ cations.[81] Other else, Cronin et al prepared a giant $\{Ce_6\}$ molybdenum blue wheel $\{Mo_{80}{}^{VI}Mo_{20}{}^{V}Ce_6{}^{III}O_{306}H_{10}(H_2O)_{70}\}^{4-}$ (Fig. 18l) by the building block rearrangement of the tetradecameric $\{Mo_{154}\}$ archetype and the control of the architecture's curvature in solution from the addition of the Ce^{3+} cation. The wheel RECP includes 10 $\{Mo_8\}$, 4 $\{Mo_2\}$, 10 $\{Mo_1\}$, 2 $\{Mo^*_1\}$, 4 $\{Ce(H_2O)_5\}$ and 2 $\{Ce(H_2O)_6\}$ groups.[17c] Furthermore, the 2-D extended architecture $[H_3RE_6(H_2O)_{26}(MoO_4)\{Mo_7O_{22}(O_2)_2\}_4]^{7-}$ (RE = Ce^{III}, Pr^{III}, Sm^{III}, Eu^{III}, Nd^{III}) (Fig. 17c) constructed from hexa-RE containing polyoxomolybdate units were also reported.[77]

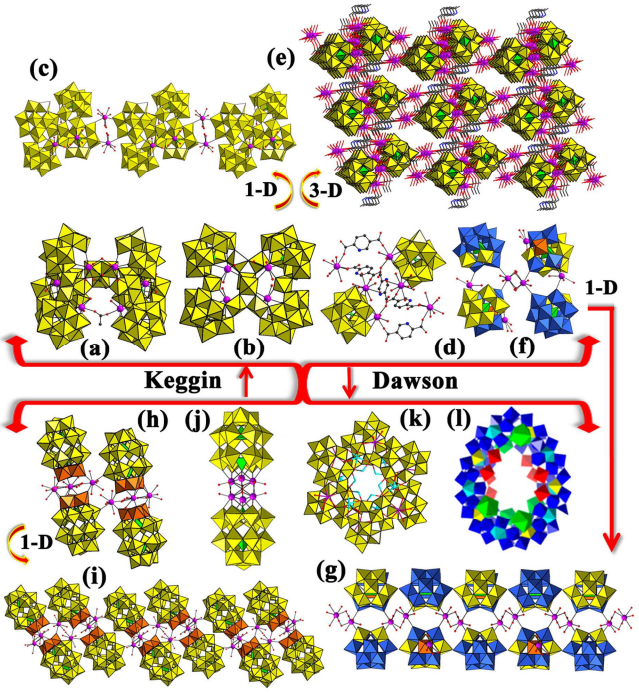

Fig. 18 (a) View of $[Gd_6As_6W_{65}O_{229}(OH)_4(H_2O)_{12}(OAc)_2]^{38-}$. (b) View of the structural unit of $[RE_6(H_2O)_x\{As_4W_{44}(OH)_2(proline)_2O_{151}\}]^{10-}$. (c) The 1-D chain of $[RE_6(H_2O)_x\{As_4W_{44}(OH)_2(proline)_2O_{151}\}]^{10-}$. (d) View of the hybrid HKRECP unit of $[RE(HL)(L)(H_2O)_6\{RE(H_2L)_{0.5}(\alpha\text{-}PW_{11}O_{39}H)RE(H_2O)_4\}]_2$. (e) The 3-D extended architecture of $[RE(HL)(L)(H_2O)_6\{RE(H_2L)_{0.5}(\alpha\text{-}PW_{11}O_{39}H)RE(H_2O)_4\}]_2$. (f) View of $[(GeW_9Nb_3O_{40})_4Eu_{5.5}(H_2O)_{26}]^{11.5-}$. (g) The 1-D chain architecture of $[(GeW_9Nb_3O_{40})_4Eu_{5.5}(H_2O)_{26}]^{11.5-}$. (h) View of $[RE_6(H_2O)_{38}(P_2W_{15}Nb_3O_{62})_4]^{18-}$. (i) The 1-D chain motif of $[RE_6(H_2O)_{38}(P_2W_{15}Nb_3O_{62})_4]^{18-}$. (j) View of $[\{Yb_6(\mu_6\text{-}O)(\mu_3\text{-}OH)_6(H_2O)_6\}(\alpha\text{-}P_2W_{15}O_{56})_2]^{14-}$. (k) View of $\{Na_{12}[(\alpha_2\text{-}P_2W_{17}O_{61}H_2)La(H_2O)_4]_6\}^{6-}$. (l) View of the giant molybdenum blue wheel RECP $\{Mo_{80}{}^{VI}Mo_{20}{}^{V}Ce_6{}^{III}O_{306}H_{10}(H_2O)_{70}\}^{4-}$ (Copied from ref. 17c). (WO_6: yellow, NbO_6: orange, W/NbO_6: blue, XO_4: bright green, RE: light purple, O: red, C: cray, N: blue, K: turquiose)

2.7 Octanuclear RECPs

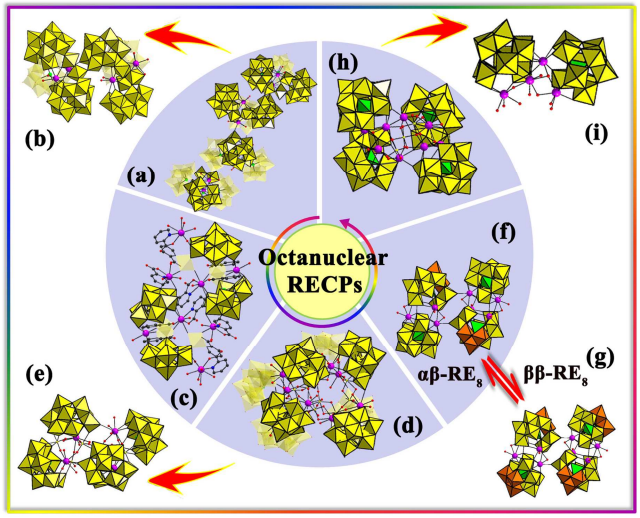

Fig. 19 (a) View of $[Gd_8As_{12}W_{124}O_{432}(H_2O)_{22}]^{60-}$. (b) View of $[Gd_4As_6W_{62}O_{216}(H_2O)_{11}]^{30-}$. (c) View of $[Tb_8(pic)_6(H_2O)_{22}(B\text{-}\beta\text{-}AsW_8O_{30})_4(WO)_2(pic))_6]^{12-}$. (d) View of $[\{(XO_3)W_{10}O_{34}\}_8\{Ce_8(H_2O)_{20}\}(WO_2)_4(W_4O_{12})]^{48-}$. (e) The half-unit $[\{(XO_3)W_{10}O_{34}\}_4\{Ce_4(H_2O)_{10}\}(WO_2)_2(W_2O_6)]^{24-}$. (f) View of $\alpha\beta\text{-}[\{RE_4(H_2O)_5(GeW_{10}O_{38})_2\}_2]^{24-}$ ($\alpha\beta\text{-}RE_8$). (g) View of $\beta\beta\text{-}[\{RE_4(H_2O)_5(GeW_{10}O_{38})_2\}_2]^{24-}$ ($\beta\beta\text{-}RE_8$). (h) The octanuclear RECPs $[(RE_2PW_{10}O_{38})_4(W_3O_8)(OH)_4(H_2O)_2]^{26-}$. (i) The packman-shaped asymmetric entity of $[(RE_2PW_{10}O_{38})_4(W_3O_8)(OH)_4(H_2O)_2]^{26-}$. To show structures more clearly, some polyhedra are faded. (WO_6: yellow and orange, XO_4: bright green, RE: light purple, O: red, C: cray, N: blue)

Historically, the first octa-Gd^{III} bridging polytungstoarsenate nanocluster $[Gd_8As_{12}W_{124}O_{432}(H_2O)_{22}]^{60-}$ (Fig. 19a) was reported by Hussain et al in 2009 by a one-pot reaction starting from a 1:2 ratio of the divacant POM $K_{14}[As_2W_{19}O_{67}(H_2O)]$ and $Gd(NO_3)_3{\cdot}6H_2O$ in NaOAc/CH_3COOH buffer at pH 4.7.[82] This nanocluster is formed by two equivalent $[Gd_4As_6W_{62}O_{216}(H_2O)_{11}]^{30-}$ (Fig. 19b) units are related by an inversion center and the $[Gd_4As_6W_{62}O_{216}(H_2O)_{11}]^{30-}$ unit can be visualized as a fusion of two equally charged trimeric units $[Gd_2As_3W_{31}O_{108}(H_2O)_6]^{15-}$ connected via W–O–W and Gd–O–W linkers. Another octanuclear RE-containing polytungstoarsenate hybrid $[Tb_8(pic)_6(H_2O)_{22}(B\text{-}\beta\text{-}AsW_8O_{30})_4(WO)_2(pic))_6]^{12-}$ (Fig. 19c) was also reported by Boskovic and collaborators through the reaction of preformed precursor $[As_2W_{19}O_{67}(H_2O)]^{14-}$.[38] Its photophysical measurements demonstrate the importance of the smaller Tb–O–W angles provided by edge- rather than corner-sharing in limiting the quenching of the organic-ligand-sensitized terbium luminescence by the POM ligands.[38] In 2013, by the precise control of the one-pot reaction, the first Ce^{III}-stabilized RECP with Se^{IV} or Te^{IV} heteroatoms $[\{(XO_3)W_{10}O_{34}\}_8\{Ce_8(H_2O)_{20}\}(WO_2)_4(W_4O_{12})]^{48-}$ (X = Se^{IV} or Te^{IV}) (Fig. 19d) was successfully separated by Wang et al, which is an octameric aggregate constructed from eight $\{(XO_3)W_{10}Ce\}$ units, four $\{WO_6\}$ octahedra and a $\{W_4\}$ unit.[17b] Alternatively, this octameric aggregate can be reckoned as the fusion of two half-units $[\{(XO_3)W_{10}O_{34}\}_4\{Ce_4(H_2O)_{10}\}(WO_2)_2(W_2O_6)]^{24-}$ (Fig. 19e). Moreover, their electrochemical activities and solution behavior were investigated.[17b] In 2014, Reinoso et al reported a family of octanuclear RECP tetramers $[\{RE_4(H_2O)_5(GeW_{10}O_{38})_2\}_2]^{24-}$ (RE = Ho^{III}, Er^{III}, Tm^{III}, Yb^{III}, Lu^{III}) (Fig. 19f, 19g), which can be assembled by the chiral $[RE_4(H_2O)_6(\beta\text{-}GeW_{10}O_{38})_2]^{12-}$ dimers when the Cs^+ cation is present.[68] More interestingly, two types of tetramers ($\beta\beta\text{-}[\{RE_4(H_2O)_5(GeW_{10}O_{38})_2\}_2]^{24-}$ and $\alpha\beta\text{-}[\{RE_4(H_2O)_5(GeW_{10}O_{38})_2\}_2]^{24-}$)

coexist in the solid state. Moreover, electronic spray ion (ESI) mass spectrometry and ^{183}W NMR spectroscopy exhibit that $[\{RE_4(H_2O)_5(GeW_{10}O_{38})_2\}_2]^{24-}$ tetramers can disassemble into $[RE_4(H_2O)_6(\beta\text{-}GeW_{10}O_{38})_2]^{12-}$ dimers upon dissolution.[68] In the same year, Hussain et al isolated a series of tetra-RE substituted tetrameric tungstophosphates $[(RE_2PW_{10}O_{38})_4(W_3O_8)(OH)_4(H_2O)_2]^{26-}$ [RE = Y^{III}, Sm^{III}, Eu^{III}, Gd^{III}, Tb^{III}, Dy^{III}, Ho^{III}, Er^{III}, Tm^{III}, Yb^{III}] (Fig. 19h) by reaction of the divacant $[P_2W_{19}O_{69}(H_2O)]^{14-}$ polyanion with $Ln(NO_3)_3\cdot nH_2O$ salts in potassium chloride solution.[83] The backbone of $[(RE_2PW_{10}O_{38})_4(W_3O_8)(OH)_4(H_2O)_2]^{26-}$ is built by four $[A\text{-}\alpha\text{-}PW_9O_{34}]^{9-}$ fragments, eight RE cations and seven additional tungsten atoms in a $[RE_8W_7O_{30}]^{6+}$ group and can be also viewed as two packman-shaped asymmetric entities (Fig. 19i) that are symmetry-related by a C_2 axis through a central tungsten atom.

2.8 Decanuclear RECPs

In 2009, Boskovic's group utilized the one-pot reactions of trivacant precursor $Na_9[B\text{-}\alpha\text{-}AsW_9O_{33}]$ and $YbCl_3\cdot 6H_2O$ in a 1 : 3 mole ratio in NaAc–HAc buffer at pH 4.7 and obtained a decanuclear RECP $[Yb_{10}As_{10}W_{88}O_{308}(OH)_8(H_2O)_{28}(OAc)_4]^{40-}$.[17a] The giant decanuclear RECP cluster is composed of eight $[B\text{-}\alpha\text{-}AsW_9O_{33}]^{9-}$ subunits, two pyramidal AsO_3 groups, twelve WO_6 octahedra, two edge-shared and acetate-bridged W_2O_{10} groups and ten Yb^{3+} cations (Fig. 20a).[17a] Its structural novelty partly arises from the incorporation of additional bridging acetate ligands that can bridge both Yb and W centers. Variable temperature magnetic susceptibility study indicates that the intramolecular magnetic exchange interactions within Yb^{3+} cations via the Yb–O–W–O–Yb pathways are negligible.[17a]

2.9 Dodecanuclear RECPs

In the past decade, only two dodeca-Ce^{III} containing POMs appeared. In 2013, Wang et al separated an unprecedented dodeca-Ce^{III} substituted selenotungstate aggregate $[\{(SeO_3)W_{10}O_{34}\}_8\{Ce_8(H_2O)_{20}\}(WO_2)_4\{(W_4O_6)Ce_4(H_2O)_{14}(SeO_3)_4(NO_3)_2\}]^{34-}$ (Fig. 20b) by the one-pot reaction of $Na_2WO_4\cdot 2H_2O$, Na_2SeO_3 and $Ce(NO_3)_3\cdot 6H_2O$.[17b] This polyoxoanionic skeleton consist of eight Keggin-type $\{(SeO_3)W_{10}Ce\}$ derivative segments, four $\{WO_6\}$ octahedra, a folded-planar-like $\{W_4\}$ group and two $\{Ce_2(NO_3)(SeO_3)_2\}$ segments. Moreover, four Ce^{3+} cations in $\{Ce_2(NO_3)(SeO_3)_2\}$ segments are well connected with the folded-planar-like $\{W_4\}$ group by SeO_3^{2-} and NO_3^- linkers. Transmission electron microscopy (TEM) study indicates that its single POAs assemble into the intact uniformsized inorganic hollow spheres in dilute water/acetone solution. In 2014, Cronin et al reported an gigantic Ce_{12}-doped decameric molybdenum blue wheel $\{Mo_{80}{}^{VI}Mo_{20}{}^{V}Ce_6{}^{III}O_{306}H_{10}(H_2O)_{71}\}_2^{8-}$ (simplified as $\{Mo_{200}Ce_{12}\}$) (Fig. 20c), which comprises two interconnected $\{Mo_{80}{}^{VI}Mo_{20}{}^{V}Ce_6{}^{III}O_{306}H_{10}(H_2O)_{70}\}^{4-}$ $\{Mo_{100}Ce_6\}$ clusters through two Ce^{3+} cations.[17c] Intriguingly, the dimeric cluster $\{Mo_{200}Ce_{12}\}$ can be transformed directly to the monomeric species $\{Mo_{100}Ce_6\}$ upon

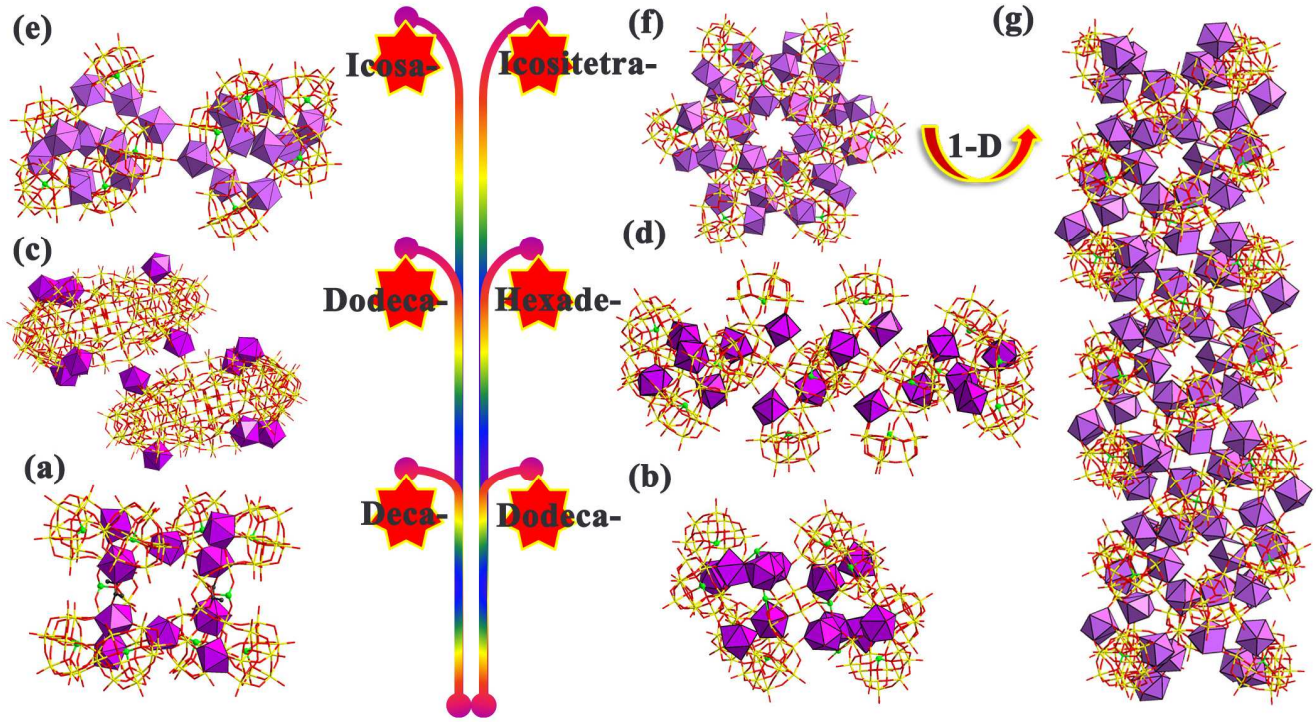

Fig. 20 (a) The decanuclear RECP $[Yb_{10}As_{10}W_{88}O_{308}(OH)_8(H_2O)_{28}(OAc)_4]^{40-}$. (b) The dodecanuclear RECP $[\{(SeO_3)W_{10}O_{34}\}_8\{Ce_8(H_2O)_{20}\}(WO_2)_4\{(W_4O_6)Ce_4(H_2O)_{14}(SeO_3)_4(NO_3)_2\}]^{34-}$. (c) The dodecanuclear RECP $\{Mo_{80}{}^{VI}Mo_{20}{}^{V}Ce_6{}^{III}O_{306}H_{10}(H_2O)_{70}\}_2^{8-}$. (d) The hexadenuclear RECP $[RE_{16}As_{16}W_{164}O_{576}(OH)_8(H_2O)_{42}]^{80-}$. (e) The icosanuclear RECP $[Ce_{20}Ge_{10}W_{100}O_{376}(OH)_4(H_2O)_{30}]^{56-}$. (f) The icositetranuclear RECP $[K\subset K_7Ce_{24}Ge_{12}W_{120}O_{456}(OH)_{12}(H_2O)_{64}]^{52-}$. (g) The 1-D alignment of $[K\subset K_7Ce_{24}Ge_{12}W_{120}O_{456}(OH)_{12}(H_2O)_{64}]^{52-}$. ($REO_x$: light purple)

addition of a potassium salt.[17c] This controllable strategy to synthesize gigantic POMs incorporating "active sites" in their anionic scaffolds allows their availability as "molecular synthons" for higher-order assembly.

2.10 Hexadecnuclear RECPs

Based on a self-assembly process of the precursor $[As_2W_{19}O_{67}(H_2O)]^{14-}$ and oxophilic RE cations, a neoteric class of hexadecnuclear RE substituted arsenotungstates $[RE_{16}As_{16}W_{164}O_{576}(OH)_8(H_2O)_{42}]^{80-}$ (RE = Eu^{III}, Gd^{III}, Tb^{III}, Dy^{III}, Ho^{III}) were isolated in alkali salt solutions (Fig. 20d).[17d] This POA can be looked on as the combination of two identical $[RE_8As_8W_{82}O_{288}(OH)_4(H_2O)_{21}]^{40-}$ asymmetric subunits by an inversion centre. Different from the reported $[Ce_{16}As_{12}(H_2O)_{36}W_{148}O_{524}]^{76-}$ POA,[84] two kinds of building blocks type-1-$[\{(AsW_9O_{33})(WO_2)(OH)\}_2]^{16-}$ and type-2-$[(AsW_9O_{33})_2W_3O_5(OH)_5]^{15-}$ coexist in the skeleton of $[RE_8As_8W_{82}O_{288}(OH)_4(H_2O)_{21}]^{40-}$ with the arrangement mode of type-1-type-2-type1-type2.

2.11 Icosanuclear RECPs

In 2007, Kortz's group obtained the 20-cerium(III)-containing 100-tungsto-10-germanate $[Ce_{20}Ge_{10}W_{100}O_{376}(OH)_4(H_2O)_{30}]^{56-}$ by the conventional reaction of the trivacant precursor $Na_{10}[\alpha\text{-}GeW_9O_{34}]$ and $CeCl_3{\cdot}7H_2O$ in a 1:1 ratio in water (pH = 5.0) (Fig. 20e).[17e] This POA can be described as a dimeric entity composed of two half units of $[Ce_{10}Ge_5W_{50}O_{188}(OH)_2(H_2O)_{15}]^{28-}$ bridged by two Ce–O(W) bonds. Each half unit contains five unprecedented dilacunary Keggin $\{\beta(4,11)\text{-}GeW_{10}O_{38}\}$ subunits connected asymmetrically by ten Ce^{3+} ions, leading to an asymmetric assembly with C_1 symmetry. Notably, this work demonstrates that the large RE cations are excellent linkers for integrating lacunary POM building blocks together to construct specific and giant assemblies.

2.12 Icositetranuclear RECPs

Inspired by indication of the icosanuclear RECP based on trivacant $[\alpha\text{-}GeW_9O_{34}]^{10-}$ building block, Reinoso and collaborators utilized the simple one-pot reaction of $Na_2WO_4{\cdot}2H_2O$, GeO_2, $Ce(NO_3)_3{\cdot}6H_2O$ and isolated the first giant crown-shaped ring icositetranuclear RECP $[K{\subset}K_7Ce_{24}Ge_{12}W_{120}O_{456}(OH)_{12}(H_2O)_{64}]^{52-}$ (Fig. 20f),[17f] which can be regarded as the product of the K^+-directed self-assembly of twelve di-Ce^{III} substituted Keggin $[Ce_2GeW_{10}O_{38}]^{6-}$ subunits. This crown-shaped POA not only comprises a unique Ce_6O_{42} central ring showing Ce^{III}–Ce^{III} antiferromagnetic interactions in which a K^+ ion is captured by internal H_2O molecules, but also demonstrates a central cavity available for ion encapsulation in an inorganic analogue of the crown ethers. In addition, adjacent $[K{\subset}K_7Ce_{24}Ge_{12}W_{120}O_{456}(OH)_{12}(H_2O)_{64}]^{52-}$ units can be combined together by Ce–O–W bridges to propagate the 1-D alignment (Fig. 20g).

3. Applications

It is well known that orbitally degenerate ground states of almost all the RE ions, apart from Gd^{III} and Eu^{II} ions with the f^7 electron configuration, are split by the spin–orbit coupling and the crystal field effect. However, due to the internal nature of 4f orbitals of RE ions, the contribution of the spin–orbit coupling is larger than the crystal-field effect to some extent, which not only greatly influences the magnetic properties of RE ions, but also provides a significant reason why RE-containing compounds hold an important position in the magnetism field.[85,86] In the past decade, the magnetic investigations on RECPs have been also performed by some researchers. The related summary is listed in Table1,[7a,17b,17d,17f,19e,21b,22,33,36,49,59–63,68,73,76,79] and several selected examples are discussed as below.

In 2013, Mizuno et al. synthesized a class of heterodinuclear RECPs $TBA_8H_4[\{Ln(\mu_2\text{-}OH)_2Ln'\}(\gamma\text{-}SiW_{10}O_{36})_2]$ (Ln = Dy^{3+}; Ln' = Eu^{3+}, Yb^{3+}, Lu^{3+}) (Fig. 4b) by the stepwise incorporation of two types of Ln cations into the vacant sites of lacunary $[\gamma\text{-}SiW_{10}O_{36}]^{8-}$ fragments and investigated their magnetic properties.[22] The alternating-current (ac) measurements under zero external field indicate that $TBA_8H_4[\{Dy(\mu_2\text{-}OH)_2Eu\}(\gamma\text{-}SiW_{10}O_{36})_2]$ (**DyEu**) and $TBA_8H_4[\{Dy(\mu_2\text{-}OH)_2Lu\}(\gamma\text{-}SiW_{10}O_{36})_2]$ (**DyLu**) exhibit the temperature- and frequency-dependent χ_m' and χ_m'' signals, explicitly revealing the SMM behavior. However, weak ac signals for $TBA_8H_4[\{Dy(\mu_2\text{-}OH)_2Yb\}(\gamma\text{-}SiW_{10}O_{36})_2]$ (**DyYb**) were seen under zero external field, may be derived from the strong quantum tunneling of magnetization that was caused by the adjacent Yb^{3+} ion. Thus, in order to inhibit the quantum tunneling of magnetization, the ac magnetic-susceptibilities of **DyYb** were measured under an external field of 1800 Oe, at this time, the temperature- and frequency-dependent χ_m' and χ_m'' signals were observed. Furthermore, their relaxation times (τ) of were obtained by the frequency dependence of the χ_m'' signals. Using the Arrhenius law ($\tau = \tau_0 \exp(\Delta E/k_BT)$) to fit the plots of ln$\tau$ versus $1/T$ afford the energy barriers for magnetization reversal ($\Delta E/k_B$) of 1.8×10^{-7} s for **DyEu**, 8.2×10^{-7} s for **DyYb**, and 1.9×10^{-6} s for **DyLu**. The energy barriers increase in the order of **DyLu < DyYb < DyEu** with an increase in the ionic radii of Ln' ions, which suggest that their energy barriers for magnetization reversal can be tuned by adjusting the coordination geometry and anisotropy of the Dy^{3+} ion and by tuning the adjacent Ln'^{3+} ion in the heterodinuclear $[Dy(\mu_2\text{-}OH)_2Ln']^{4+}$ cores.

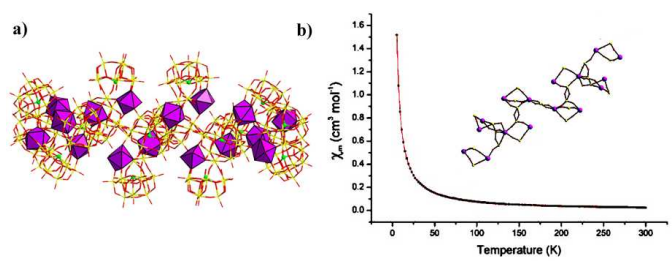

Fig. 21 (a) The structure of hexadenuclear RECP $[Gd_{16}As_{16}W_{164}O_{576}(OH)_8(H_2O)_{42}]^{80-}$. (b) Temperature-dependent of magnetic susceptibility recorded between 5 K and 300 K (inset: ball-and-stick representation of the connection mode of Gd^{3+} centers) (Copied from ref. 17d).

In 2011, Patzke et al. measured the variable-temperature magnetic susceptibility of $[Gd_{16}As_{16}W_{164}O_{576}(OH)_8(H_2O)_{42}]^{80-}$ from 5 K to 300 K in an applied magnetic field of 2000 Oe with respect to the presence of sixteen Gd^{3+} centers (Fig. 21).[17d] As it is a paramagnetic system without orbital contribution, the curve of magnetic susceptibility can be fitted by using the follow equation:

$$\chi = [N\beta^2 g^2 S(S+1)/3kT] + \chi_{dia}$$

Here, g is defined as 2.0, the resulting χ_{dia} value is 0.0034 emu·mol^{-1} (χ_{dia} denotes the diamagnetic correction) and the resulting spin value S was 3.468. The χ_{dia} value is in good agreement with the value for diamagnetic

susceptibility calculated from Pascal constants. The spin value corresponds to the spin of non-interacting Gd^{3+} ions (S = 7/2), and is in consistence with the large Gd–Gd distances from 5.9 to 6.3 Å because of the indirect linking through O–W–O bridges.

On the other hand, RE-doped materials are of great interest for a wide range of potential applications in light-emitting diodes, tunable lasers, sensory probes, fluorescent tubes, plasma displays, etc.[87–89] These unique application functionalities can be ascribed to the narrow emission and high color purity generated from the RE ions.[91] Additionally, RE ions are often subjected to weak light absorption owing to the forbidden f–f transitions, entailing the direct excitation of RE ions to be very inefficient if high-power laser excitation isn't used. This difficulty can be surmounted by the luminescence sensitization or antenna effect.[91a,92] Thus, the photoluminescence properties of some RECPs have been also investigated at room temperature (Table 1).[21,39,44,51,59,61,68,69,73,77,78,80] For example, Zhao and co-workers probed the solid-state photoluminescence behavior of $Na_{10}[Tb_2(C_2O_4)(H_2O)_4(OH)W_4O_{16}]_2\cdot 30H_2O$ at room temperature.[73] The emission spectrum upon excitation at 369 nm exhibits four groups of bands at 490, 495 nm; 543, 545 nm; 584, 588 nm; and 621 nm, which can be respectively assigned to $^5D_4\rightarrow{}^7F_6$, $^5D_4\rightarrow{}^7F_5$, $^5D_4\rightarrow{}^7F_4$, and $^5D_4\rightarrow{}^7F_3$ transitions of Tb^{3+} cations (Fig. 22a). By monitoring Tb^{3+} $^5D_4\rightarrow{}^7F_5$ emission at 543 nm, its excitation spectrum displays a broadband between 250 and 350 nm that is originated from the absorption of $[W_4O_{16}]^{8-}$ segment, indicating that the luminescence emission partly comes from the contribution of POM-centered ligand-to-metal charge-transfer (LMCT) process. This phenomenon somewhat differs from the observation in $[Tb_8(pic)_6(H_2O)_{22}(B\text{-}\beta\text{-}AsW_8O_{30})_4(WO_2(pic))_6]^{12-}$,[38] and the result reported by Yamase[13a]. Moreover, its decay behavior conforms to a biexponential function as $I = A_1\exp(-t/\tau_1) + A_2\exp(-t/\tau_2)$, affording lifetimes of τ_1 = 0.43 ms and τ_2 = 1.25 ms (Fig. 22b). This behavior is analogous to that of those hydrated Tb^{III} complexes,[38,93] which also coincides with the case that each Tb^{3+} cation is coordinated by two water ligands based on the single-crystal structural analysis of $Na_{10}[Tb_2(C_2O_4)(H_2O)_4(OH)W_4O_{16}]_2\cdot 30H_2O$. Liu's group investigated the solid-state photoluminescence behavior of $Cs_3K_4[(Ge_2W_{18}Nb_6O_{78})Eu(H_2O)_4]\cdot 23H_2O$ at room temperature.[69] Five characteristic emission bands located at 579, 592, 614, 651 and 699 nm are seen and correspond to the $^5D_0\rightarrow{}^7F_0$, $^5D_0\rightarrow{}^7F_1$, $^5D_0\rightarrow{}^7F_2$, $^5D_0\rightarrow{}^7F_3$ and $^5D_0\rightarrow{}^7F_4$ transitions of Eu^{3+} ions, respectively (Fig. 22c). In general, the $^5D_0\rightarrow{}^7F_0$ transition is symmetry-forbidden in a field of symmetry. But the $^5D_0\rightarrow{}^7F_0$ transition is seen here, revealing that the site symmetry of the Eu^{3+} is low in $Cs_3K_4[(Ge_2W_{18}Nb_6O_{78})Eu(H_2O)_4]\cdot 23H_2O$. Furthermore, the $I(^5D_0\rightarrow{}^7F_2)/I(^5D_0\rightarrow{}^7F_1)$ radio is 7.25, which also supports this point. Moreover, its solution photoluminescence behavior was also probed and the solution emission spectrum manifests the uniform manner to the solid-state emission spectrum, suggesting the uniform coordination environments of Eu^{3+} ions in the solid and solution states. The luminescence response experiments to various carboxylic acids such as acetate, oxalic, malonic and succinic acids have been performed. The results illustrate that the emission intensity significantly rises upon the addition of malonic acid while the introduction of other three carboxylic acids does not lead to obvious changes to the emission spectra (Fig. 22d). This luminescent response may be interpreted by the substitution of coordinated water molecules by the polarizable C–O donors of the malonic acid in solution state.[69,94]

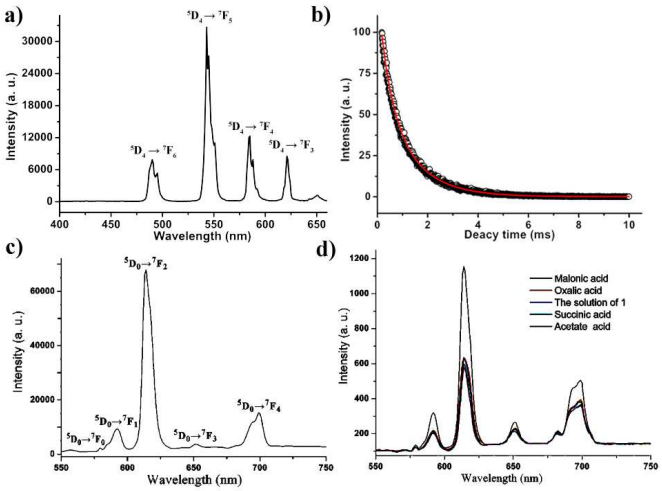

Fig. 22 (a) The emission spectrum (λ_{ex} = 369 nm) of $Na_{10}[Tb_2(C_2O_4)(H_2O)_4(OH)W_4O_{16}]_2\cdot 30H_2O$ (Copied from ref. 73 with some changes). (b) The luminescence decay curve of $Na_{10}[Tb_2(C_2O_4)(H_2O)_4(OH)W_4O_{16}]_2\cdot 30H_2O$ (Copied from ref. 69 with some changes). (c) The emission spectrum (λ_{ex} = 394 nm) of solid-state $Cs_3K_4[(Ge_2W_{18}Nb_6O_{78})Eu(H_2O)_4]\cdot 23H_2O$ (Copied from ref. 69 with some changes). (d) The luminescence spectra of $Cs_3K_4[(Ge_2W_{18}Nb_6O_{78})Eu(H_2O)_4]\cdot 23H_2O$ (1.0×10^{-3} mol·L^{-1}, in 0.5 mol·L^{-1} HCl solution) upon addition of acetate acid, oxalic acid, malonic acid and succinic acids (1.0 equal, λ_{ex} = 394 nm) (Copied from ref. 69 with some changes).

Apart from above-mentioned magnetic and luminescence properties of RECPs, other application explorations such as Lewis acid–base catalysis, photocatalysis, electrocatalysis, photochromism, ferroelectric properties etc have been also involved in this field (Table 1).[42, 79, 80, 61, 21c] These properties are not discussed here.

4. Summary and outlook

In the past decade, a large number of inorganic or organic–inorganic hybrid RECPs with diverse structures and interesting properties have been prepared and excavated due to the driving force originating from their intriguing applications ranging from catalysis to magnetism. These systematic and profound researches on RECPs not only gradually highlight and underline an important place of the RECP branch in the frontier area of POM chemistry, but also can provide the great valuable guidance to the ongoing and continuous developments of exploring and discovering novel functional RECPs. Obviously, during the course of preparing RECPs, the conventional solution approach is the most useful and efficient method, however, the hydrothermal technique very little involves. In the conventional solution system, initial reactants, pH value, reaction time, temperature and the selection of solvent are often considered as the important reaction parameters in controlling the possibility of reaction and affecting the formation and crystal growth of the product phases. In addition to these various parameters, the judicious option of synthetic strategies is a crucial factor. Hitherto, some effective synthetic strategies such as the one-pot reaction strategy of simple starting materials, the adaptive POM precursors as the starting building blocks, the mixed solvent method, the buffer solution control with appropriate pH range, the alkali metal-directed self-assembly, and the

Table 1 Summary of applications of some RECPs.

Formula	RE	Properties	Ref
$Na_{15.69}Cs_{15.31}H_9[Yb_{10}As_{10}W_{88}O_{308}(OH)_8(H_2O)_{28}(OAc)_4]\cdot 84H_2O$	Yb^{3+}	the decrease of $\chi_m T$ with decreasing temperature is due to the thermal depopulation of higher multiplet states	17a
$K_{32}Na_{16}[\{(SeO_3)W_{10}O_{34}\}_8\{Ce_8(H_2O)_{20}\}(WO_2)_4(W_4O_{12})]\cdot 81H_2O$	Ce^{3+}	the dominant antiferromagnetic interactions	17b
$Na_{55}K_{14}Cs_{11}[Gd_{16}As_{16}W_{164}O_{576}(OH)_8(H_2O)_{42}]\cdot nH_2O$ (n≈220)	Gd^{3+}	the single ion behavior	17d
$Na_{40}K_6[Ni(H_2O)_6]_3[K\subset K_7Ce_{24}Ge_{12}W_{120}O_{456}(OH)_{12}(H_2O)_{64}]\cdot n H_2O$ (n≈178)	Ce^{3+}	the antiferromagnetic interactions	17f
$[Sm(H_2O)_6]_{0.25}[Sm(H_2O)_5]_{0.25}H_{0.5}\{Sm(H_2O)_7[Sm(H_2O)_2(DMSO)(\alpha\text{-}SiW_{11}O_{39})]\}\cdot 4.5H_2O$	Sm^{3+}	the coexistence of strong spin-orbital coupling interactions and very weak ferromagnetic responses	19e
$TBA_8H_4[\{RE(\mu_2\text{-}OH)_2RE'\}(\gamma\text{-}SiW_{10}O_{36})_2]$	RE = Dy^{3+}; RE'= Eu^{3+}, Yb^{3+}, Lu^{3+}	the single molecule magnet behavior	22
$[(CH_3)_4N]_6[\{(\alpha\text{-}PW_{11}O_{39}H)Nd(H_2O)_3\}_2]_3\ 8H_2O$ $[(CH_3)_4N]_{10}[\{(\alpha\text{-}PW_{11}O_{39})Sm(H_2O)(\eta^2,\mu\text{-}1,1)\text{-}CH_3COO\}_2]_3\ 6H_2O$	Nd^{3+}, Sm^{3+}	the coexistence of the spin-orbital coupling interactions and weak antiferromagnetic exchange interactions	33
$[C(NH_2)_3]_{11}[Dy_2(Hcit)_2(AsW_{10}O_{38})]\cdot 9H_2O$	Dy^{3+}	the weak antiferromagnetic coupling interactions and the thermal depopulation of the Dy^{3+} excited states	36
$Na_{22}[(BiW_9O_{33})_4(WO_3)\{Bi_6(\mu_3\text{-}O)_4(\mu_2\text{-}OH)_3\}(Pr_3(H_2O)_6CO_3)]\cdot 95H_2O$	Pr^{3+}	the progressive depopulation of excited Stark sublevels of the Pr^{3+} ions at low temperature and the weak antiferromagnetic interactions	59
$K_{13}H_4Li[Ho_2(C_4H_4O_6)(C_4H_2O_6)(AsW_9O_{33})]_2\cdot 28H_2O$	Ho^{3+}	the progressive depopulation of excited Stark sublevels of the Ho^{3+} ions at low temperature and the weak antiferromagnetic interactions	62
$(HDABCO)_8H_5Li_8[Tb_4As_5W_{40}O_{144}(H_2O)_{10}(gly)_2]_3\ 25H_2O$	Tb^{3+}	the single molecule magnet behavior	63
$Na_{12}[Dy_4(H_2O)_6(\beta\text{-}GeW_{10}O_{38})_2]\ \approx 44H_2O$	Dy^{3+}	the single molecule magnet behavior	68
$Na_{10}[Eu_2(C_2O_4)(H_2O)_4(OH)W_4O_{16}]_2\cdot 30H_2O$	Eu^{3+}	the declining of $\chi_m T$ upon cooling prevailingly originates from the progressive depopulation of the excited state of Eu^{3+} cations	73
$K_4Na_{16}[Ho(C_2O_4)W_5O_{18}]_4\cdot 60H_2O$	Ho^{3+}	the antiferromagnetic coupling interactions within HoIII centers and thermal depopulation of the Stark sublevels of the Ho^{3+} cation	73
$[CeK(H_2O)_{12}][Ce(H_2O)_6]_2[(H_2O)_4CeBW_{11}O_{39}H]_2\cdot 20H_2O$	Ce^{3+}	the declining of $\chi_m T$ upon cooling is due to the depopulation of the higher Stark levels of the Ce^{3+} ions	76a
$KCe[(H_2O)_6Ce]_2[(H_2O)_4CeSiW_{11}O_{39}]_2\cdot 40H_2O$	Ce^{3+}	the declining of $\chi_m T$ upon cooling is due to the depopulation of the higher Stark levels of the Ce^{3+} ions	76b
$[Ce(HL)(L)(H_2O)_6\{Ce(H_2L)_{0.5}(\alpha\text{-}PW_{11}O_{39}H)Ce(H_2O)_4\}]_2\cdot 12H_2O$ (H_2L=2,5-pyridine dicarboxylic acid)	Ce^{3+}	the antiferromagnetism coupling interactions	79
$K_{11}[Eu(PW_{11}O_{39})_2]\cdot xH_2O$	Eu^{3+}	red photoluminescence excitation peak: 460 nm emission peaks: $^5D_0\rightarrow{}^7F_0$ (582 nm), $^5D_0\rightarrow{}^7F_1$ (596 nm), $^5D_0\rightarrow{}^7F_2$ (616 nm), $^5D_0\rightarrow{}^7F_3$ (652 nm) and $^5D_0\rightarrow{}^7F_4$ (704 nm)	21a
$Na_4K_8[\{Tb(\alpha\text{-}SiW_{11}O_{39})(H_2O)\}_2(\mu\text{-}CH_3COO)_2]\cdot 22H_2O$	Tb^{3+}	green photoluminescence excitation peak: 330 nm emission peaks: $^5D_4\rightarrow{}^7F_5$ (546 nm), $^5D_4\rightarrow{}^7F_4$ (584 nm) and $^5D_4\rightarrow{}^7F_3$ (623 nm)	21b
$KNa_3[HPro]_7[Sm(\alpha\text{-}PW_{11}O_{39})_2]\cdot Pro\cdot 18H_2O$	Sm^{3+}	excitation peak: 410 nm emission peaks: $^4G_{5/2}\rightarrow{}^6H_{5/2}$ (555 nm), $^4G_{5/2}\rightarrow{}^6H_{7/2}$ (595 nm) and $^4G_{5/2}\rightarrow{}^6H_{9/2}$ (620 nm)	21c
$K_4Li_4H_4[Tb_8(pic)_6(H_2O)_{22}(B\text{-}\beta\text{-}AsW_8O_{30})_4(WO)_2(pic))_6]\cdot 58H_2O$	Tb^{3+}	green photoluminescence excitation peak: 275 nm emission peaks: $^5D_4\rightarrow{}^7F_6$ (492 nm), $^5D_4\rightarrow{}^7F_5$ (544 nm), $^5D_4\rightarrow{}^7F_4$ (583 nm) and $^5D_4\rightarrow{}^7F_3$ (623 nm)	39
$(H_2bpy)_2[Eu_2(H_2O)_9(\alpha_2\text{-}P_2W_{17}O_{61})]\cdot 5H_2O$	Eu^{3+}	excitation peak: 398 nm emission peaks: $^5D_0\rightarrow{}^7F_0$ (578 nm), $^5D_0\rightarrow{}^7F_1$ (591 nm), $^5D_0\rightarrow{}^7F_2$ (648 nm) and $^5D_0\rightarrow{}^7F_3$ (696 nm)	44

Table 1 continuted.

Formula	RE	Properties	Ref
$[Na_2(H_2O)_2K_5(H_2O)_6][H_6Ce_2(H_2O)ClW_{15}O_{54}]\cdot 6H_2O$	Ce^{3+}	blue photoluminescence excitation peak: 264nm emission peaks: 5d→$^2F_{5/2}$ (488 nm)	51
$Na_{22}[(BiW_9O_{33})_4(WO_3)\{Bi_6(\mu_3\text{-}O)_4(\mu_2\text{-}OH)_3\}(Pr_3(H_2O)_6CO_3)]\cdot 95H_2O$	Pr^{3+}	excitation peak: 230 nm emission peaks: $^1S_0 \rightarrow {}^1I_6$ (411 nm), $^3H_4 \rightarrow {}^1D_2$ (464 nm), f–f transitions of $^3P_0 \rightarrow {}^3H_4$ (480 nm, 492nm)	59
$Na_4Cs_3DyH[Dy_2(H_2O)_{6.5}(C_2H_4O_2)_{0.5}Si_2W_{18}O_{66}]Cl_3\ 17H_2O$	Dy^{3+}	excitation peak: 357nm emission peaks: $^4F_{9/2} \rightarrow {}^6H_{15/2}$ (479 nm) and $^4F_{9/2} \rightarrow {}^6H_{13/2}$ (574 nm)	61
$Na_{12}[Dy_4(H_2O)_6(\beta\text{-}GeW_{10}O_{38})_2] \approx 44H_2O$	Dy^{3+}	yellow photoluminescence excitation peak: 325 nm emission peaks: $^4F_{9/2}\rightarrow{}^6H_{15/2}$ (485 nm), $^4F_{9/2}\rightarrow{}^6H_{13/2}$ (573 nm) and $^4F_{9/2}\rightarrow{}^6H_{11/2}$ (663 nm).	68
$Cs_3K_4[(Ge_2W_{18}Nb_6O_{78})Eu(H_2O)_4]\ 23H_2O$	Eu^{3+}	excitation peak: 394 nm emission peaks: $^5D_0\rightarrow{}^7F_0$ (579 nm), $^5D_0\rightarrow{}^7F_1$ (592 nm), $^5D_0\rightarrow{}^7F_2$ (614 nm), $^5D_0\rightarrow{}^7F_3$ (651 nm) and $^5D_0\rightarrow{}^7F_4$ (699 nm) solution photoluminescence behavior: selective luminescence response to malonic acid	69
$Na_{10}[Tb_2(C_2O_4)(H_2O)_4(OH)W_4O_{16}]_2\cdot 30H_2O$	Tb^{3+}	excitation peak: 369 nm emission peaks: $^5D_4\rightarrow{}^7F_6$ (490 nm, 495 nm), $^5D_4\rightarrow{}^7F_5$ (543 nm, 545 nm), $^5D_4\rightarrow{}^7F_4$ (584 nm, 588 nm) and $^5D_4\rightarrow{}^7F_3$ (621 nm)	73
$Na_2(NH_4)_3[H_3Sm_6(H_2O)_{26}(MoO_4)\{Mo_7O_{22}(O_2)_2\}_4]\cdot 24H_2O$	Sm^{3+}	excitation peak: 435 nm emission peaks: $^4G_{5/2} \rightarrow {}^6H_{5/2}$ (551 nm), $^4G_{5/2} \rightarrow {}^6H_{7/2}$ (570 nm), and $^4G_{5/2} \rightarrow {}^6H_{9/2}$ (653 nm)	77
$Na_{10}[Tb_6(H_2O)_{22}\{As_4W_{44}(OH)_2(proline)_2O_{151}\}]\cdot 22H_2O$	Tb^{3+}	green photoluminescence excitation peak: 348 nm emission peaks: $^5D_4\rightarrow{}^7F_6$ (490 nm), $^5D_4\rightarrow{}^7F_5$ (544 nm), $^5D_4\rightarrow{}^7F_4$ (586 nm) and $^5D_4\rightarrow{}^7F_3$ (621 nm)	78
$K_6Na_4H_8[Eu_6(H_2O)_{38}(P_2W_{15}Nb_3O_{62})_4]\cdot 45H_2O$	Eu^{3+}	excitation peak: 394 nm emission peaks: $^5D_0\rightarrow{}^7F_0$ (579 nm), $^5D_0\rightarrow{}^7F_1$ (591 nm), $^5D_0\rightarrow{}^7F_2$ (613 nm), $^5D_0\rightarrow{}^7F_3$ (653 nm) and $^5D_0\rightarrow{}^7F_4$ (699 nm)	80
$KNa_3[HPro]_7[Sm(\alpha\text{-}PW_{11}O_{39})_2]\cdot Pro\cdot 18H_2O$	Sm^{3+}	the ferroelectric behavior	21c
$Na_2[(CH_3)_2NH_2]_3\{Na\subset[Ce^{III}(H_2O)(CH_3CH_2OH)(L\text{-}tartH_3)(H_2Si_2W_{19}O_{66})]\}\cdot 3.5H_2O$ $[(CH_3)_2NH_2]_7\{Na\subset[Ce^{III}(H_2O)(CH_3CH_2OH)(D\text{-}tartH_3)(Si_2W_{19}O_{66})]\}\cdot 2.5H_2O$	Ce^{3+}	two-photon absorption properties typical of the third-order nonlinear optical response	29
$TBA_6H_4[\{RE(H_2O)_2\cdot n(acetone)\}_2\{\gamma\text{-}SiW_{10}O_{36}\}_2]\cdot 2H_2O$	Gd^{3+}	the Lewis acid–base catalysis for cyanosilylation	42
$Na_4Cs_3Ho[Ho_2(H_2O)_7Si_2W_{18}O_{66}]_3\ 18H_2O$	Ho^{3+}	the photochromic behavior	61
$[La(HL)(L)(H_2O)_6\{La(H_2L)_{0.5}(\alpha\text{-}PW_{11}O_{39}H)La(H_2O)_4\}]_2\cdot 8H_2O$ (H_2L = 2,5-pyridinedicarboxylic acid)	La^{3+}	the photocatalytical degradation of the rhodamine-B	79
$K_6Na_4H_8[Ce_6(H_2O)_{38}(P_2W_{15}Nb_3O_{62})_4]\cdot 56H_2O$	Ce^{3+}	the good electrocatalytic activity towards the reduction of nitrite	80

inducing reaction strategy of the lone electron pair stereochemical effect of some heteroatoms have been constantly and intensively utilized and attempted in the preparations of RECPs. These synthetic strategies have been involved in the above-mentioned discussion. Above all, this review primarily concentrates on the elaborate statements about novel structures from mononuclear RECPs to icositetranuclear RECPs. We put emphasis on illuminating structural characteristics, the linking or assembly modes of different compositions and structural types of different building blocks in some representative examples. Certainly, some interesting or important properties are also concerned at the same time.

The area of POMs is currently entering into a new phase whereby it is possible to design and control both the structures and functionalities of the systems.[95] On base of the previous results and our critical comprehensions, several personal insights or viewpoints are presented here to help researchers that are engaged in this domain to understand the frontiers of RECP science and grasp the future development direction of neoteric RECPs. Meanwhile, we hope to motivate others to step into this area bringing in new ideas and perspectives.

(i) From the viewpoint of synthetic chemistry, in view of the fact that the hydrothermal reaction is seldom used to prepare RECPs, as a result, the extension of the synthetic approach from the conventional solution

system to the hydrothermal reaction system will favor to the discovery of novel RECP hybrids accompanying the introduction of some functional components and can also result in the formation of unseen non-equilibrium POM fragments and unexpected functionalities that are not accessible from the near equilibrium environments under the conventional solution conditions.

(ii) As a hotspot research field of inorganic chemistry, the chiral POM-based materials have attracted extensive interest while relevant reports about chiral RECPs are sparse, which suggests that introducing appropriate chiral ligands (including inorganic and organic) to the RECP system to produce chiral RECPs will be an emerging area that bears potential applications in asymmetric catalysis, nonlinear optic, gas separation and molecular recognition.

(iii) The exploration and discovery of much higher nuclear RE incorporated POM aggregations or nanoclusters remains a great and severe challenge albeit an icositetranuclear RECP has been isolated because the encapsulation of much more RE cations to the POM matrixes can enhance and tune the magnetic, luminescent or bifunctional catalytic performances of high-nuclear RECPs.

(iv) To date, the majority of reported RECPs are purely inorganic, which inevitably entails the synthesis and study of organic–inorganic hybrid RECPs to become a new research topic. Whereby, multi-functional organic ligands (e. g. polycarboxylic ligands, aminoacids, etc) will be brought in the reaction system to construct organic–inorganic hybrid RECP clusters or high-dimensional frameworks. In addition, by virtue of the antenna effect of functional organic ligands can in some degree overcome or improve the low absorptivity of RE cations in the ultraviolet-visible region and sensitize the emission of RE cations, thus enhance the luminous efficiency of RE cations.

Acknowledgements

This work was supported by the Natural Science Foundation of China (21301049, U1304208, 21571048), the Natural Science Foundation of Henan Province (122300410106), the Postdoctoral Foundation of Henan Province, 2014 Special Foundation for Scientific Research Project of Henan University, 2012 Young Backbone Teachers Foundation from Henan Province (2012GGJS-027) and the Students Innovative Pilot Plan of Henan University (15NA002).

Abbreviations

POM	Polyoxometalate
POA	Polyoxoanion
RE	Rare earth
TM	Transition metal
Ln	Lanthanide
TMSP	Transition metal substituted polyoxometalate
RECP	Rare-earth containing polyoxometalate
HSAB	Hard and Soft Acids and Bases theory
MKRECP	Mononuclear Keggin-type RECP
MDRECP	Mononuclear Dawson-type RECP
MLRECP	Mononuclear Lindqvist-type RECP
DKRECP	Dinuclear Keggin-type RECP
DDRECP	Dinuclear Dawson-type RECP
DARECP	Dinuclear Anderson-type RECP
TKRECP	Trinuclear Keggin-type RECP
TDLECP	Trinuclear Dawson-type RECP
QKRECP	Quadrnuclear Keggin-type RECP
QDRECP	Quadrnuclear Dawson-type RECP
QLRECP	Quadrnuclear Lindqvist-type RECP
PKRECP	Pentanuclear Keggin-type RECP
PDRECP	Pentanuclear Dawson-type RECP
HKRECP	Hexanuclear Keggin-type RECP
HDRECP	Hexanuclear Dawson-type RECP
CD	circular dichroism
SMM	Single molecule magnet
pro	proline
$tartH_4$	tartaric acid
ala	L-α-alanine
DMF	N,N-Dimethylformamide
TBA	Tetra-n-butylammonium
DMSO	Dimethyl sulfoxide
Hpic	4-picolinic acid
$C_6H_5NO_2$	Pyridine-4-carboxylic acid
HAc	Acetic acid
acac	acetylacetonato
H_4cit	Citric acid
H_3CAM	2,6-Dicarboxy-4-hydroxypyridine
gly	glycine
Nle	Norleucine
H_2pydc	Pyridine-2,3-dicarboxylic acid
TEM	Transmission electron microscopy

Notes and references

Henan Key Laboratory of Polyoxometalate Chemistry, Institute of Molecular and Crystal Engineering, College of Chemistry and Chemical Engineering, Henan University, Kaifeng, Henan 475004, P. R. China. E-mail: zhaojunwei@henu.edu.cn, ljchen@henu.edu.cn, Fax: (+86) 371 23886876.

1 (*a*) A. Dolbecq, E. Dumas, C. R. Mayer and P. Mialane, *Chem. Rev.*, 2010, **110**, 6009; (*b*) H. N. Miras, L. Vilà-Nadal and L. Cronin, *Chem. Soc. Rev.*, 2014, **43**, 5679; (*c*) C. L. Hill and C. M. Prosser-McCartha, *Coord. Chem. Rev.*, 1995, **143**, 407.
2 B. S. Bassil and U. Kortz, *Z. Anorg. Allg. Chem.*, 2010, **636**, 2222.
3 (*a*) M. T. Pope, *Heteropoly and Isopoly Oxometalates,* Springer, Berlin, 1983; (*b*) E.-B. Wang, C.-W. Hu and L. Xu, *Introduction of Polyacid Chemistry*, Chemical Industry Press, Beijing, 1998; (*c*) L. C. W. Baker and D. C. Glick, *Chem. Rev.*, 1998, **98**, 3.
4 M. T. Pope and A. Müller, *Angew. Chem., Int. Ed. Engl.*, 1991, **30**, 34.
5 (*a*) C. L. Hill, *Chem. Rev.*, 1998, **98**, 1; (*b*) D. L. Long, E. Burkholder and L. Cronin, *Chem. Soc. Rev.*, 2007, **36**, 105.
6 (*a*) X. Fang, P. Kögerler, Y. Furukawa, M. Speldrich and M. Luban, *Angew. Chem. Int. Ed.*, 2011, **50**, 5212; (*b*) Y. Kikukawa, Y. Kuroda, K. Yamaguchi and N. Mizuno, *Angew. Chem. Int. Ed.*, 2012, **51**, 2434; (*c*) H. J. Lv, Y. V. Geletii, C. C. Zhao, J. W. Vickers, G. B. Zhu, Z. Luo, J. Song, T. Q. Lian, D. G. Musaev and C. L. Hill, *Chem. Soc. Rev.*, 2012, **41**, 7572; (*d*) S.-T. Zheng and G.-Y. Yang, *Chem. Soc. Rev.*, 2012, **41**, 7623; (*e*) L. Cronin and A. Müller, *Chem. Soc. Rev.*, 2012, **41**, 7333; (*f*) J. M. Clemente-Juan, E. Coronado and A. Gaita-Ariño, *Chem. Soc. Rev.*, 2012, **41**, 7464; (*g*) S.-S. Wang and G.-Y. Yang, *Chem. Rev.*, 2015, **115**, 4893.
7 (*a*) J. Berzelius, *Pogg. Ann.*, 1826, **6**, 369; (*b*) J. F. Keggin, *Proc. R. Soc. London Ser.*, 1934, **A144**, 75.
8 Y. Z. Li, J. Luo, L. J. Chen and J. W. Zhao, *RSC Adv.*, 2014, **4**, 50679.

9 G. A. Barbieri, *Atti. Accad. Nazi. Lincei*, 1914, **11**, 805.
10 (*a*) R. D. Peacock and T. J. R. Weakley, *J. Chem. Soc. A*, 1971, 1836; (*b*) R. D. Peacock and T. J. R. Weakley, *J. Chem. Soc. A*, 1971, 1937.
11 (*a*) V. E. Simmons, L.C.W. Baker, *Proc. VII I.C.C.C.*, *Stockholm*, 1962, 195; (*b*) L. C. W. Baker, V. E. Simmons, *Proc. IX I.C.C.C.*, *St. Moritz*, 1966, 421.
12 (*a*) M. T. Pope, *Compr. Coord. Chem. II,* 2003, **4**, 635; (*b*) C. L. Hill, *Compr. Coord. Chem. II*, 2003, **4**, 679; (*c*) J. J. Borras-Almenar, E. Coronado, A., Müller and M. T. Pope, *Polyoxometalate Molecular Science,* Kluwer: Dordrecht, The Netherlands, 2004.
13 (*a*) T. Yamase, *Chem. Rev.*, 1998, **98**, 307; (*b*) C. Benelli and D. Gatteschi, *Chem. Rev.*, 2002, **102**, 2369; (*c*) H. E. Moll, B. Nohra, P. Mialane, J. Marrot, N. Dupré, B. Riflade, M. Malacria, S. Thorimbert, B. Hasenknopf, E. Lacôte, P. A. Aparicio, X. López, J. M. Poblet and A. Dolbecq, *Chem. Eur. J.*, 2011, **17**, 14129; (*d*) Y. Kikukawa, S. Yamaguchi, K. Tsuchida, Y. Nakagawa, K. Uehara, K. Yamaguchi and N. Mizuno, *J. Am. Chem. Soc.*, 2008, **130**, 5472; (*e*) C. Boglio, G. Lemière, B. Hasenknopf, S. Thorimbert, E. Lacôte and M. Malacria, *Angew. Chem. Int. Ed.*, 2006, **45**, 3324.
14 (*a*) L. Armelao, S. Quici, F. Barigelletti, G. Accorsi, G. Bottaro, M. Cavazzini and E. Tondello, *Coord. Chem. Rev.*, 2010, **254**, 487; (*b*) B. A. Hess, A. Kedziorski, L. Smentek and D. J. Bornhop, *J. Phys. Chem. A*, 2008, **112**, 2397; (c) J.-C. G. Bünzli, A.-S. Chauvin, C. D. B. Vandevyver, B. Song and S. Comby, *Ann. N. Y. Acad. Sci.*, 2008, **1130**, 97; (*d*) K. Binnemans, *Chem. Rev.*, 2009, **109**, 4283.
15 R. G. Pearson, *J. Am. Chem. Soc.*, 1963, **85**, 3533.
16 V. Chandrasekhar, P. Bag and E. Colacio, *Inorg. Chem.*, 2013, **52**, 4562.
17 (*a*) F. Hussain, R. Gable, M. Speldrich, P. Kögerler and C. Boskovic, *Chem. Commun.*, **2009**, 328; (*b*) W. C. Chen, H. L. Li, X. L. Wang, K.-Z. Shao, Z. M. Su and E. B. Wang, *Chem. Eur. J.*, 2013, **19**, 11007; (*c*) W. M. Xuan, A. J. Surman, H. N. Miras, D. L. Long and L. Cronin, *J. Am. Chem. Soc.*, 2014, **136**, 14114; (*d*) F. Hussain and G. R. Patzke, *CrystEngComm*, 2011, **13**, 530; (*e*) B. S. Bassil, M. H. Dickman, I. Römer, B. Kammer and U. Kortz, *Angew. Chem. Int. Ed.*, 2007, **46**, 6192; (*f*) S. Reinoso, M. Giménez-Marqués, J. Galán-Mascarós, P. Vitoria and J. M. Gutiérrez-Zorrilla, *Angew. Chem. Int. Ed.*, 2010, **49**, 8384.
18 M. Fedotov, B. Pertsikov and D. Kanovich, *Polyhedron*, 1990, **9**, 1249.
19 M. Sadakane, M. H. Dickman and M. T. Pope, *Angew. Chem. Int. Ed.*, 2001, **39**, 2914.
20 (*a*) P. Mialane, L. Lisnard, A. Mallard, J. Marrot, E. Antic-Fidancev, P. Aschehoug, D. Vivien and F. Sécheresse, *Inorg. Chem.*, 2003, **6**, 2102; (*b*) J. Y. Niu, J. W. Zhao and J. P. Wang, *Inorg Chem Comm.*, 2004, **7**, 876; (*c*) J. P. Wang, J. W. Zhao and J. Y. Niu, *Sci. China, Ser. B,* 2005, **48**, 343; (*d*) J. P. Wang, X. Y. Duan, X. D. Du and J. Y. Niu, *Cryst. Growth Des.*, 2006, **6**, 2266; (*e*) J. P. Wang, J. W. Zhao, X. Y. Duan and J. Y. Niu, *Cryst. Growth Des.*, 2006, **6**, 507.
21 (*a*) R. Gupta, M. K. Saini, F. Doungmene, P. de Oliveira and F. Hussain, *Dalton Trans.*, 2014, **43**, 8290; (*b*) M. K. Saini, R. Gupta, S. Parbhakar, A. K. Mishra, R. Mathurb and F. Hussain, *RSC Adv.*, 2014, **4**, 25357; (*c*) Y. J. Liu, H. L. Li, J. L. Zhang, J. W. Zhao and L. J. Chen, *Spectrochim. Acta Part A: Mol. Biomol. Spectr.*, 2015, **134**, 101.
22 R. Sato, K. Suzuki, M. Sugawa and N. Mizuno, *Chem. Eur. J.*, 2013, **19**, 12982.
23 A. H. Ismail, B. S. Bassil, I. Römer and U. Kortz, *Z. Anorg. Allg. Chem.*, 2013, **639**, 2510.
24 (*a*) B. Hasenknopf, K. Micoine, E. Lacôte, S. Thorimbert, M. Malacria and R. Thouvenot, *Eur. J. Inorg. Chem.*, 2008, 5001; (*b*) C. Boglio, K. Micoine, P. Rémy, B. Hasenknopf, S. Thorimbert, E. Lacôte, M. Malacria, C. Afonso and J.-C. Tabet, *Chem. Eur. J.*, 2007, **13**, 5426; (*c*) K. Micoine, B. Hasenknopf, S. Thorimbert, E. Lacôte and M. Malacria, *Angew. Chem., Int. Ed.*, 2009, **48**, 3466.
25 B. S. Bassil, M. H. Dickman, B. Kammer and U. Kortz, *Inorg. Chem.*, 2007, **46**, 2452.
26 H. Naruke, J. Iijia and T. Sanji, *Inorg. Chem.*, 2011, **50**, 7535.
27 N. Belai, M. H. Dickman, M. T. Pope, R. Contant, B. Keita, I. M. Mbomekalle and L. Nadjo, *Inorg. Chem.*, 2005, **44**, 169.
28 H. L. Li, W. Yang, Y. Chai, L. L. Chen and J. W. Zhao, *Inorg Chem Comm.*, 2015, **56**, 35.
29 W. W. Ju, H. T. Zhang, X. Xu, Y. Zhang and Y. Xu, *Inorg. Chem.*, 2014, **53**, 3269.
30 V. Shivaiah, P. V. Narasimha Reddy, L. Cronin and S. K. Das, *J. Chem. Soc., Dalton Trans.*, 2002, 3781.
31 V. Shivaiah, T. Chatterjee and S. K Das, *J. Chem. Sci.*, 2014, **126**, 1525.
32 C. Liu, F. Luo, N. Liu, Y. Cui, X. Wang, E. B. Wang and J. Chen, *Cryst. Growth Des.*, 2006, **6**, 2658.
33 J. Y. Niu, K. H. Wang, H. N. Chen, J. W. Zhao, P. T. Ma, J. P. Wang, M. X. Li, Y. Bai and D. B. Dang, *Cryst. Growth Des.*, 2009, **9**, 4362.
34 S. W. Zhang, Y. Wang, J. W. Zhao, P. T. Ma, J. P. Wang and J. Y. Niu, *Dalton Trans.*, 2012, **41**, 3764.
35 J. P. Wang, J. W. Zhao, X. Y. Duan and J. Y. Niu, *Cryst. Growth Des.*, 2006, **6**, 507.
36 F. Y. Li, W. H. Guo, L. X u, L. F. Ma and Y. C. Wang, *Dalton Trans.*, 2012, **41**, 9220.
37 (*a*) S.-T. Zheng, J. Zhang, X.-X. Li, W.-H. Fang and G.-Y. Yang, *J. Am. Chem. Soc.,* 2010, **132**, 15102; (*b*) S.-T. Zheng, J. Zhang and G.-Y. Yang, *Angew. Chem. Int. Ed.* 2008, **47**, 3909.
38 C. Ritchie, E. G. Moore, M. Speldrich, P. Kögerler and C. Boskovic, *Angew. Chem. Int. Ed.*, 2010, **49**, 7702.
39 (*a*) U. Kortz, A. Müller, J. Slageren, J. Schnack, N. S. Dalal and M. Dressel, *Coord. Chem. Rev.*, 2009, **253**, 2315; (*b*) M. Bosco, S. Rat, N. Dupré, B. Hasenknopf, E. Lacote, M. Malacria, P. Rémy, J. Kovensky, S. Thorimbert and A. Wadouachi, *ChemSusChem*, 2010, **3**, 1249.
40 N. Dupré, P. Rémy, K. Micoine, C. Boglio, S. Thorimbert, E. Lacôte, B. Hasenknopf and M. Malacria, *Chem. Eur. J.*, 2010, **16**, 7256.
41 K. Suzuki, M. Sugawa, Y. Kikukawa, K. Kamata, K. Yamaguchi and N. Mizuno, *Inorg. Chem.*, 2012, **51**, 6953.
42 C. Boglio, G. Lenoble, C. Duhayon, B. Hasenknopf, R. Thouvenot, C. Zhang, R. C. Howell, B. P. Burton-Pye, L. C. Francesconi, E. Lacôte, S. Thorimbert, M. Malacria, C. Afonso and J.-C. Tabet, *Inorg. Chem.*, 2006, **45**, 1389.
43 Y. Lu, Y. Xu, Y. G. Li, E. B. Wang, X. X. Xu and Y. Ma, *Inorg. Chem.*, 2006, **45**, 2055.
44 M. Zimmermann, N. Belai, R. J. Butcher, M. T. Pope, E. V. Chubarova, M. H. Dickman and U. Kortz, *Inorg. Chem.*, 2007, **46**, 1737.
45 (*a*) D. Drewes, E. M. Limanski and B. Krebs, *Eur. J. Inorg. Chem.,* 2004, 4849; (*b*) D. Drewes and B. Krebs, *Z. Anorg. Allg. Chem.*, 2005, **631**, 2591.
46 H. Y. An, Y. G. Li, D. R. Xiao, E. B. Wang and C. Y. Sun, *Cryst. Growth Des.*, 2006, **6**, 1107.
47 X. J. Kuang and I. R. Evans, *Inorg. Chem.*, 2010, **49**, 6005.
48 (*a*) H. N. Miras, J. Yan, D. L. Long and L. Cronin, *Angew. Chem. Int. Ed.*, 2008, **47**, 8420; (*b*) J. Fuchs, R. Palm and H. Hartl, *Angew. Chem. Int. Ed. Engl.*, 1996, **35**, 2651; (*c*) T. Lehmann and J. Z. Z. Fuchs, *Naturforsch. B*, 1988, **43**, 89; (*d*) R. Singer and H. Gross, *Helv. Chim. Acta*, 1934, **17**, 1076.
49 X. T. Zhang, D. Q. Wang, J. M. Dou, S. S. Yan, X. X. Yao and J. Z. Jiang, *Inorg. Chem.*, 2006, **45**, 10629.
50 T. H. Li, F. Li, J. Lü, Z. G. Guo, S. Y. Gao and R. Cao, *Inorg. Chem.*, 2008, **47**, 5612.
51 A. H. Ismail, B. S. Bassil, A. Suchopar and U. Kortz, *Eur. J. Inorg. Chem.*, 2009, 5247.
52 A. H. Ismail, M. H. Dickman, and U. Kortz, *Inorg. Chem.*, 2009, **48**, 1559.
53 W. C. Chen, X. L. Wang, Y. Q. Jiao, P. Huang, E. L. Zhou, Z. M. Su, and K. Z. Shao, *Inorg. Chem.*, 2014, **53**, 9486.
54 T. Arumuganathan and S. K. Das, *Inorg. Chem.*, 2009, **48**, 496.
55 (*a*) W. Chen, Y. Li, Y. Wang, E. B. Wang and Z. Zhang, *Dalton Trans.*, 2008, 865; (*b*) F. Hussain, B. Spingler, F. Conrad, M. Speldrich, P. Kögerler, C. Boskovic and G. Patzke, *Dalton Trans.*, 2009, **1**, 4423.
56 C. Ritchie and C. Boskovic, *Cryst. Growth Des.*, 2010, **10**, 488.
57 M. Ibrahim, S. S. Mal, B. S. Bassil, A. Banerjee and U. Kortz, *Inorg. Chem.*, 2011, **50**, 956.
58 I. Loose, E. Droste, M. Bösing, H. Pohlmann, M. H. Dickman, C. Rosu, M. T. Pope and B. Krebs, *Inorg. Chem.*, 1999, **38**, 2688.
59 K. Y. Cui, F. Y. Li, L. Xu, B. B. Xu, N. Jiang, Y. C. Wang and J. P. Zhang, *Dalton Trans.*, 2012, **41**, 4871.
60 (*a*) M. Mirzaei, H. Eshtiagh-Hosseini, N. Lotfian, A. Salimi, A. Bauzá, R. V. Deun, R. Decadt, M. Barceló-Oliver and A. Frontera, *Dalton Trans.*, 2014, **43**, 1906; (*b*) N. Lotfian, M. Mirzaei, H. Eshtiagh-Hosseini, M. Löffler, M. Korabik and A. Salimi, *Eur. J. Inorg. Chem.*, 2014, 5908.
61 L. B. Ni, F. Hussain, B. Spingler, S. Weyeneth and G. Patzke, *Inorg. Chem.*, 2011, **50**, 4944.

62 Y. Wang, X. P. Sun, S. Z. Li, P. T. Ma, J. P. Wang and J. Y. Niu, *Dalton Trans.*, 2015, **44**, 733.
63 C. Ritchie, M. Speldrich, R. W. Gable, L. Sorace, P. Kögerler and C. Boskovic, *Inorg. Chem.*, 2011, **50**, 7004.
64 M. Vonci, F. A. Bagherjeri, P. D. Hall, R. W. Gable, A. Zavras, R. A. J. O'Hair, Y. P. Liu, J. Zhang, M. R. Field, M. B. Taylor, J. D. Plessis, G. Bryant, M. Riley, L. Sorace, P. A. Aparicio, X. López, J. M. Poblet, C. Ritchie, and C. Boskovic, *Chem. Eur. J.*, 2014, **20**, 14102.
65 S. Z. Li, Y. Wang, P. T. Ma, J. P. Wang and J. Y. Niu, *CrystEngComm*, 2014, **16**, 10746.
66 (*a*) W. L. Chen, Y. G. Li, Y. H. Wang, E. B. Wang and Z. M. Su, *Dalton Trans.*, 2007, 4293; (*b*) K. Wassermann and M. T. Pope, *Inorg. Chem.*, 2001, **40**, 2763; (*c*) A. Müller, M. T. Pope, A. Merca, H. Bge, M. Schmidtmann, J. V. Slageren, M. Dressel and D. G. Kurth, *Chem. Eur. J.*, 2005, **11**, 5849.
67 Y. G. Li, L. Xu, G. G. Gao, N. Jiang, H. Liu, F. Y. Li and Y. Y. Yang, *CrystEngComm*, 2009, **11**, 1512.
68 B. Artetxe, S. Reinoso, L. S. Felices, L. Lezama, J. M. Gutiérrez-Zorrilla, J. A. García, J. R. Galán-Mascarós, A. Haider, U. Kortz and C. Vicent, *Chem. Eur. J.*, 2014, **20**, 12144.
69 S. J. Li, S. X. Liu, N. N. Ma, Y. Q. Qiu, J. Miao, C. C. Li, Q. Tang and L, Xu, *CrystEngComm*, 2012, **14**, 1397.
70 R. X. Tan, X. H. Pang, Y. L. Ren, X. H. Wang and R. Li, *Z. Anorg. Allg. Chem.*, 2011, **637**, 1178.
71 X. K. Fang, T. M. Anderson, C. Benelli and C. L. Hill, *Chem. Eur. J.*, 2005, **11**, 712.
72 L. Huang, L. Cheng, W. H. Fang, S. S. Wang and G. Y. Yang, *Eur. J. Inorg. Chem.*, 2013, 1693.
73 J. W. Zhao, H. L. Li, Y. Z. Li, C. Y. Li, Z. L. Wang and L. J. Chen, *Cryst. Growth Des.*, 2014, **14**, 5495.
74 L. Y. Song, D. D. Zhang, P. T. Ma, Z. J. Liang, J. P. Wang and J. Y. Niu, *CrystEngComm*, 2013, **15**, 4597.
75 D. Drewes, M. Piepenbrink and B. Krebs, *Z. Anorg. Allg. Chem.*, 2006, **632**, 534.
76 (*a*) H. Y. An, Z. B. Han and T. Q. Xu, *Inorg. Chem.*, 2010, **49**, 11403; (*b*) H. Y. An, H. Zhang, Z. F. Chen, Y. G. Li, X. Liu and H. Chen, *Dalton Trans.*, 2012, **41**, 8390.
77 J. J. Wei, L. Yang, P. T. Ma, J. P. Wang and J. Y. Niu, *Cryst. Growth Des.*, 2013, **13**, 3554.
78 X. J. Feng, H. Y. Han, Y. H. Wang, L. L. Li, Y. G. Li and E. B. Wang, *CrystEngComm*, 2013, **15**, 7267.
79 K. Wang, D. D. Zhang, J. C. Ma, P. T. Ma, J. Y. Niu and J. P. Wang, *CrystEngComm*, 2012, **14**, 3205.
80 C. C. Li, S. X. Liu, S. J. Li, Y. Yang, H. Y. Jin and F. J. Ma, *Eur. J. Inorg. Chem.*, 2012, 3229.
81 S. W. Zhang, D. D. Zhang, P. T. Ma, Y. F. Liang, J. P. Wang and J. Y. Niu, *CrystEngComm*, 2013, **15**, 2992.
82 F. Hussain, F. Conrad and G. R. Patzke, *Angew. Chem. Int. Ed.*, 2009, **48**, 9088.
83 R. Gupta, M. Saini and F. Hussain, *Eur. J. Inorg. Chem.*, 2014, 6031.
84 L. M. Rodriguez-Albelo, A. R. Ruiz-Salvador, A. Sampieri, D. W. Lewis, A. Gomez, B. Nohra, P. Mialane, J. Marrot, F. Sécheresse, C. Mellot-Draznieks, R. N. Biboum, B. Keita, L. Nadjo and A. Dolbecq, *J. Am. Chem. Soc.*, 2009, **131**, 16078.
85 C. Benelli and D. Gatteschi, *Chem. Rev.*, 2002, **102**, 2369.
86 M. L. Kahn, J.-P. Sutter, S. Golhen, P. Guionneau, L. Ouahab, O. Kahn, and D. Chasseau, *J. Am. Chem. Soc.*, 2000, **122**, 3413.
87 E. Soini and I. Hemmilä, *Clin. Chem.*, 1979, **25**, 353.
88 L. Armelao, S. Quici, F. Barigelletti, G. Accorsi, G. Bottaro, M. Cavazzini and E. Tondello, *Coord. Chem. Rev.*, 2010, **254**, 487.
89 J. C. G. Buünzli and C. Piguet, *Chem. Soc. Rev.,* 2005, **34**, 1048.
90 S. V. Eliseevaa and J.-C. G. Bünzli, *Chem. Soc. Rev.*, 2010, **39**, 189.
91 (*a*) Y. Cui, Y. Yue, G. Qian and B. Chen, *Chem. Rev.*, 2012, **112**, 1126; (*b*) Y. Li, F.-K. Zheng, X. Liu, W.-Q. Zou, G.-C. Gou, C.-Z. Lu and J.-S. Huang, *Inorg. Chem.*, 2006, **45**, 6308.
92 (*a*) B. D. Chandler, D. T. Cramb and G. K. H. Shimizu, *J. Am. Chem. Soc.*, 2006, **128**, 10403; (*b*) E. G. Moore, A. P. S. Samuel and K. N. Raymond, *Acc. Chem. Res.*, 2009, **42**, 542; (*c*) N. Sabbatini, M. Guardigli and J.-M. Lehn, *Coord. Chem. Rev.*, 1993, **123**, 201.
93 (*a*) C. Ritchie, V. Baslon, E. G. Moore, C. Reber and C. Boskovic, *Inorg. Chem.,* 2012, **51**, 1142; (*b*) D. L. Rosen and S. Niles, *Appl. Spectrosc.*, 2001, **55**, 208.
94 (*a*) B. L. Chen, S. C. Xiang and G. D. Qian, *Acc. Chem. Res.*, 2010, **43**, 1115; (*b*) J. I. Bruce, R. S. Dickins, L. J. Govenlock, T. Gunnlaugsson, S. Lopinski, M. P. Lowe, D. Parker, R. D. Peacock, J. J. B. Perry, S. Aime and M. Botta, *J. Am. Chem. Soc.*, 2000, **122**, 9674.
95 H. N. Miras, J. Yan, D.-L. Long and L. Cronin, *Chem. Soc. Rev.*, 2012, **41**, 7403.

Graphic Abstract

Significant developments on rare-earth-containing polyoxometalate chemistry: synthetic strategies, structural diversities and correlative properties

Xing Ma, Wen Yang, Lijuan Chen* and Junwei Zhao*